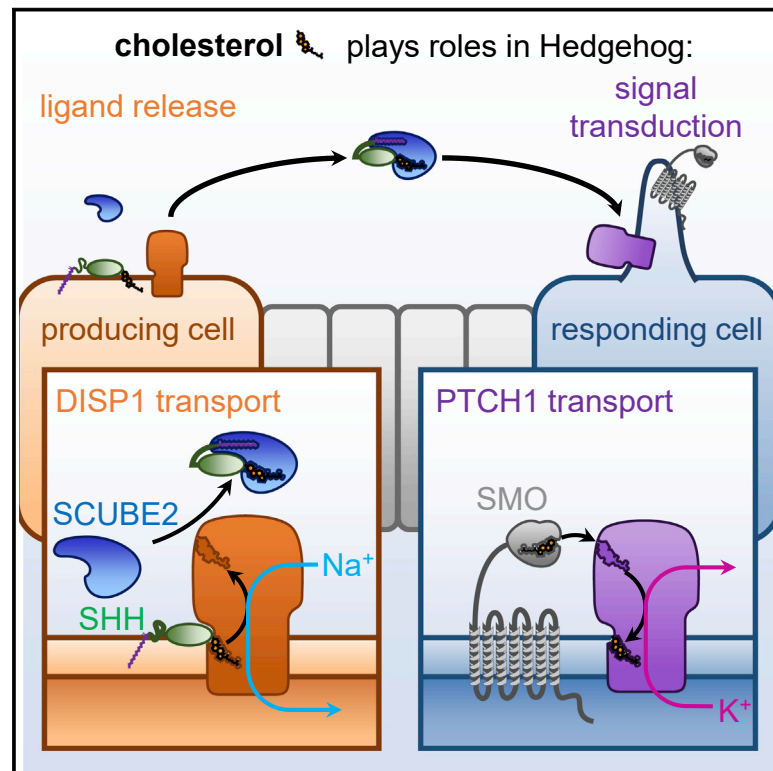


Developmental Cell

Distinct Cation Gradients Power Cholesterol Transport at Different Key Points in the Hedgehog Signaling Pathway

Graphical Abstract



Authors

Kostadin Petrov,
Bradley M. Wierbowski, Jingjing Liu,
Adrian Salic

Correspondence

asalic@hms.harvard.edu

In Brief

Petrov, Wierbowski et al. show that eukaryotic RND proteins Dispatched1 and Patched1, key regulators of the Hedgehog developmental signaling pathway, are transporters powered by distinct ion gradients across the plasma membrane: Dispatched1 uses Na⁺ to catalyze cholesterol-modified Sonic hedgehog secretion, whereas Patched1 uses K⁺ to antagonize Smoothened activation by cholesterol.

Highlights

- The Hedgehog pathway RND proteins DISP1 and PTCH1 are cation-powered transporters
- DISP1 uses the transmembrane Na⁺ gradient to catalyze cholesterylated SHH secretion
- PTCH1 uses the transmembrane K⁺ gradient to block SMO activation by cholesterol
- Key residue conservation suggests how ion fluxes couple to substrate transport

Article

Distinct Cation Gradients Power Cholesterol Transport at Different Key Points in the Hedgehog Signaling Pathway

Kostadin Petrov,^{1,3} Bradley M. Wierbowski,^{1,3} Jingjing Liu,^{1,2} and Adrian Salic^{1,4,*}

¹Department of Cell Biology, Harvard Medical School, 240 Longwood Avenue, Boston, MA 02115, USA

²School of Life Sciences, Peking University, 5 Yiheyuan Road, Beijing 100871, China

³These authors contributed equally

⁴Lead Contact

*Correspondence: asalic@hms.harvard.edu

<https://doi.org/10.1016/j.devcel.2020.08.002>

SUMMARY

Cholesterol plays two critical roles in Hedgehog signaling, a fundamental pathway in animal development and cancer: it covalently modifies the Sonic hedgehog (SHH) ligand, restricting its release from producing cells, and directly activates Smoothed in responding cells. In both contexts, a membrane protein related to bacterial RND transporters regulates cholesterol: Dispatched1 controls release of cholesterylated SHH, and Patched1 antagonizes Smoothed activation by cholesterol. The mechanism and driving force for eukaryotic RND proteins, including Dispatched1 and Patched1, are unknown. Here, we show that Dispatched1 acts enzymatically to catalyze SHH release. Dispatched1 uses the energy of the plasma membrane Na⁺ gradient, thus functioning as an SHH/Na⁺ antiporter. In contrast, Patched1 repression of Smoothed requires the opposing K⁺ gradient. Our results clarify the transporter activity of essential eukaryotic RND proteins and demonstrate that the two main cation gradients of animal cells differentially power cholesterol transport at two crucial steps in the Hedgehog pathway.

INTRODUCTION

The Hedgehog (Hh) signaling pathway is essential in embryogenesis of most metazoans (Ingham and McMahon, 2001; Lum and Beachy, 2004), while aberrant Hh activity is responsible for several cancers, including basal cell carcinoma and medulloblastoma (Rubin and de Sauvage, 2006). When the Hh pathway is not stimulated, the membrane protein Patched1 (PTCH1) (Nakano et al., 1989) inhibits the GPCR-like protein Smoothed (SMO) (Alcedo et al., 1996; van den Heuvel and Ingham, 1996), thus ensuring that the downstream Hh pathway is idle. Signaling is initiated by a secreted Hedgehog ligand, such as the vertebrate prototype, Sonic hedgehog (SHH) (Chang et al., 1994; Echelard et al., 1993; Krauss et al., 1993; Riddle et al., 1993). SHH binds and inhibits PTCH1, allowing SMO to become active. Active SMO then triggers activation of the downstream zinc finger GLI proteins (Humke et al., 2010; Tukachinsky et al., 2010), which turn on transcription of specific target genes.

A unique aspect of Hh signaling is the critical involvement of cholesterol at two distinct steps (Figure 1A). First, in signal-producing cells, cholesterol is covalently attached to SHH (Porter et al., 1996), causing it to strongly associate with membranes; thus, cholesterol is crucial for regulating SHH production and distribution. Second, in responding cells, cholesterol activates SMO (Huang et al., 2016; Luchetti et al., 2016) by binding to its

extracellular cysteine-rich domain (CRD) (Byrne et al., 2016; Huang et al., 2016; Myers et al., 2013; Nachtergaele et al., 2013; Nedelcu et al., 2013); thus, cholesterol is required for Hh signal transduction (Cooper et al., 2003).

Each of the two cholesterol-dependent aspects in Hh signaling involves a protein related to the resistance–nodulation–division (RND) superfamily of transporters (Nikaido, 2018). In signal-producing cells (Figure 1B), the RND-related Dispatched1 (DISP1) (Amanai and Jiang, 2001; Burke et al., 1999; Caspary et al., 2002; Kawakami et al., 2002; Ma et al., 2002; Nakano et al., 2004) is necessary for SHH release in a diffusible form capable of long-distance signaling. DISP1 interacts with the cholesteryl moiety of SHH (Creanga et al., 2012; Tukachinsky et al., 2012), transferring it from the membrane to a secreted SCUBE family protein, such as SCUBE2 (Hollway et al., 2006; Kawakami et al., 2005; Woods and Talbot, 2005). In Hh-responding cells (Figure 4A), PTCH1, itself RND-related, is thought to inhibit SMO by transporting cholesterol. The idea that cholesterol is the PTCH1 substrate is supported by the observation of sterol molecules in recent cryo-EM structures of PTCH1 (Gong et al., 2018; Qi et al., 2018a, 2018b; Qian et al., 2019; Zhang et al., 2018), although the manner and direction of the presumed cholesterol movement are unclear.

The RND superfamily includes both prokaryotic and eukaryotic members. Prokaryotic RNDs function as proton (H⁺)-driven

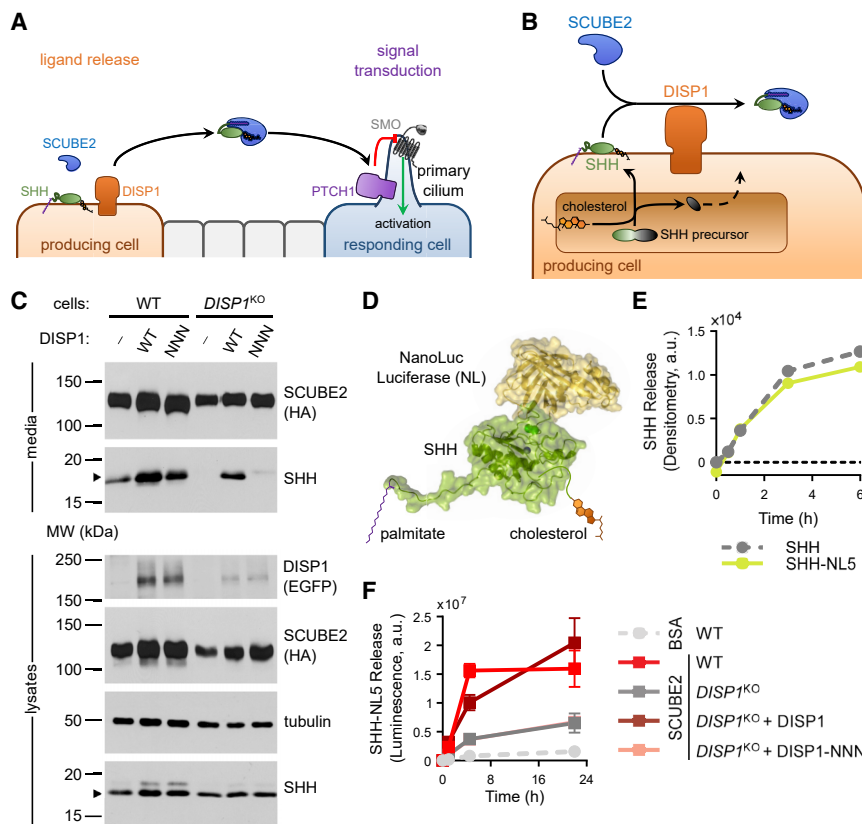


Figure 1. Reconstitution of DISP1-Dependent SHH Release in Cultured Cells

(A) Schematic of the Hh signaling pathway, showing the two RND-related proteins, DISP1 and PTCH1, which play essential roles in SHH ligand release and in signal transduction, respectively. (B) DISP1 is required for the release of SHH as a soluble complex with a SCUBE family protein. Whether DISP1 acts as a catalytic transporter of cholesterylated SHH, and how DISP1 is powered, are open questions.

(C) Wild-type or *DISP1* knockout (*DISP1*^{KO}) HEK293T cells were co-transfected with SHH, HA-tagged SCUBE2, and the indicated EGFP-tagged DISP1 constructs. SHH release into serum-free media was assayed by immunoblotting. SHH is not released in the absence of DISP1, which is reversed by wild-type DISP1, but not by the inactive DISP1-NNN mutant. Arrowheads indicate the band corresponding to dually lipid-modified SHH. (D) Schematic of the SHH-NL5 fusion (PDB: 6e1h.c and 5ibo).

(E) SHH-NL5 or SHH was stably expressed in HEK293T cells, and release by purified SCUBE2 (500 nM) was measured by anti-SHH immunoblotting and densitometry. Released amounts were normalized to the level of SHH species in each cell line. SHH-NL5 and untagged SHH are released with similar kinetics. See also [Figures S1G–S1J](#) for blots and luminescence measurements.

(F) SHH-NL5 was stably expressed in wild-type or *DISP1*^{KO} HEK293T cells, and SHH-NL5 release by purified SCUBE2 (300 nM) into serum-free media was measured by luminescence. SHH-NL5

release by bovine serum albumin (BSA, 300 nM) served as a negative control. Defective SHH-NL5 release in *DISP1*^{KO} cells is rescued by expression of wild-type DISP1, but not by the inactive DISP1-NNN mutant. Data represent the mean of two biological replicates and error bars show standard deviation around the mean. See also [Figure S1](#) for characterization of SHH-NL fusions and for recombinant SCUBE2 purification.

antiporters in which expulsion of small-molecule substrates from the periplasm of Gram-negatives to the extracellular space is coupled with inward H⁺ flow, from the periplasm into the cytoplasm (Aires and Nikaido, 2005; Delmar et al., 2015; Seeger et al., 2006). Eukaryotic RND-related proteins include Niemann-Pick disease protein C1 (NPC1) (Carstea et al., 1997) and NPC1L1 (Davis et al., 2004), which play fundamental roles in cholesterol metabolism, and DISP1 and PTCH1, which are essential for embryonic development. In contrast to bacterial RNDs, however, eukaryotic RND-related proteins remain poorly understood mechanistically. Catalytic substrate transport has not been directly demonstrated for any eukaryotic RND, and, furthermore, it is unknown if and how eukaryotic RNDs are powered by ionic gradients. Two residues required for H⁺ conductance in bacterial RNDs are conserved and required for DISP1 (Ma et al., 2002) and PTCH1 (Taipale et al., 2002) function; in the case of PTCH1, mutations in these residues cause Gorlin syndrome, a genetic predisposition to cancers caused by hyperactive Hh signaling (Taipale et al., 2002). However, unlike bacteria, most eukaryotic cells do not maintain an H⁺ gradient across the plasma membrane, suggesting that eukaryotic RNDs, including DISP1 and PTCH1, perhaps rely on different ionic gradients. A recent report suggested that PTCH1 activity requires the Na⁺ gradient (Myers et al., 2017), but this study was not per-

formed in Hh-responsive cells and did not use a physiological Hh readout, leaving the issue of how PTCH1 is powered in cells undergoing normal Hh signaling unresolved.

Here, we address two major open questions concerning eukaryotic RND-related proteins: do they catalyze substrate transport, and what is their energy source? We start by developing a fast and quantitative assay for DISP1 activity, which we use to demonstrate that DISP1 acts catalytically to transport cholesterylated SHH during its release from cells. We find that the plasma membrane Na⁺ gradient is absolutely required for DISP1 activity, while the K⁺ gradient is dispensable; furthermore, increasing the steepness of the Na⁺ gradient potentiates DISP1 activity. Since cholesterylated SHH is released to the extracellular space while Na⁺ enters the cell, this indicates that DISP1 functions as a Na⁺-powered antiporter. In contrast, in the case of PTCH1, we find that its inhibitory effect on SMO requires the K⁺ gradient but not the Na⁺ gradient; this suggests that PTCH1 operates as a K⁺-powered cholesterol transporter. Both for DISP1 and PTCH1, mutagenesis and functional assays support the role of a cation different from H⁺. Our results demonstrate catalytic transporter activity for a crucial eukaryotic RND and show that the two critical steps in the Hh pathway involving cholesterol transport are powered by two distinct monovalent cationic gradients across the plasma membrane.

RESULTS

A Quantitative Cellular System for DISP1-Dependent SHH Release

Despite the critical importance of eukaryotic RND-related proteins, catalytic transporter function has not been directly demonstrated for any of them. To tackle this problem, we focused on developing a biochemical system for measuring DISP1 activity. The choice of DISP1 was based on the following rationales: (1) DISP1 functions at the plasma membrane, thus is immediately accessible to factors added exogenously; (2) the movement of the cholesterylated SHH substrate is well-defined, from the outer membrane leaflet to the extracellular SCUBE2 acceptor; and (3) uniquely among eukaryotic RNDs, DISP1 acts on a cholesterol substrate attached to a protein, which should greatly simplify quantification (Figure 1B).

SHH release by SCUBE2 has been observed in cultured HEK293T cells (Creanga et al., 2012; Tukachinsky et al., 2012), but it is unclear if this process requires endogenous DISP1. We thus generated *DISP1* knockout (*DISP1*^{KO}) HEK293T cells (Figure S1A) and measured SHH release. As shown in Figure 1C, SCUBE2 did not release SHH from *DISP1*^{KO} cells, in contrast to the robust release observed in parental wild-type cells. Importantly, SCUBE2-dependent SHH release was fully rescued by transfecting *DISP1*^{KO} cells with a construct expressing wild-type DISP1 but not the inactive DISP1-NNN mutant (Ma et al., 2002) (Figure 1C), indicating the specificity of the SHH release defect. Thus, SHH release from HEK293T cells recapitulates the strict requirement for DISP1 and SCUBE family proteins observed in *in vivo* studies of the Hh pathway.

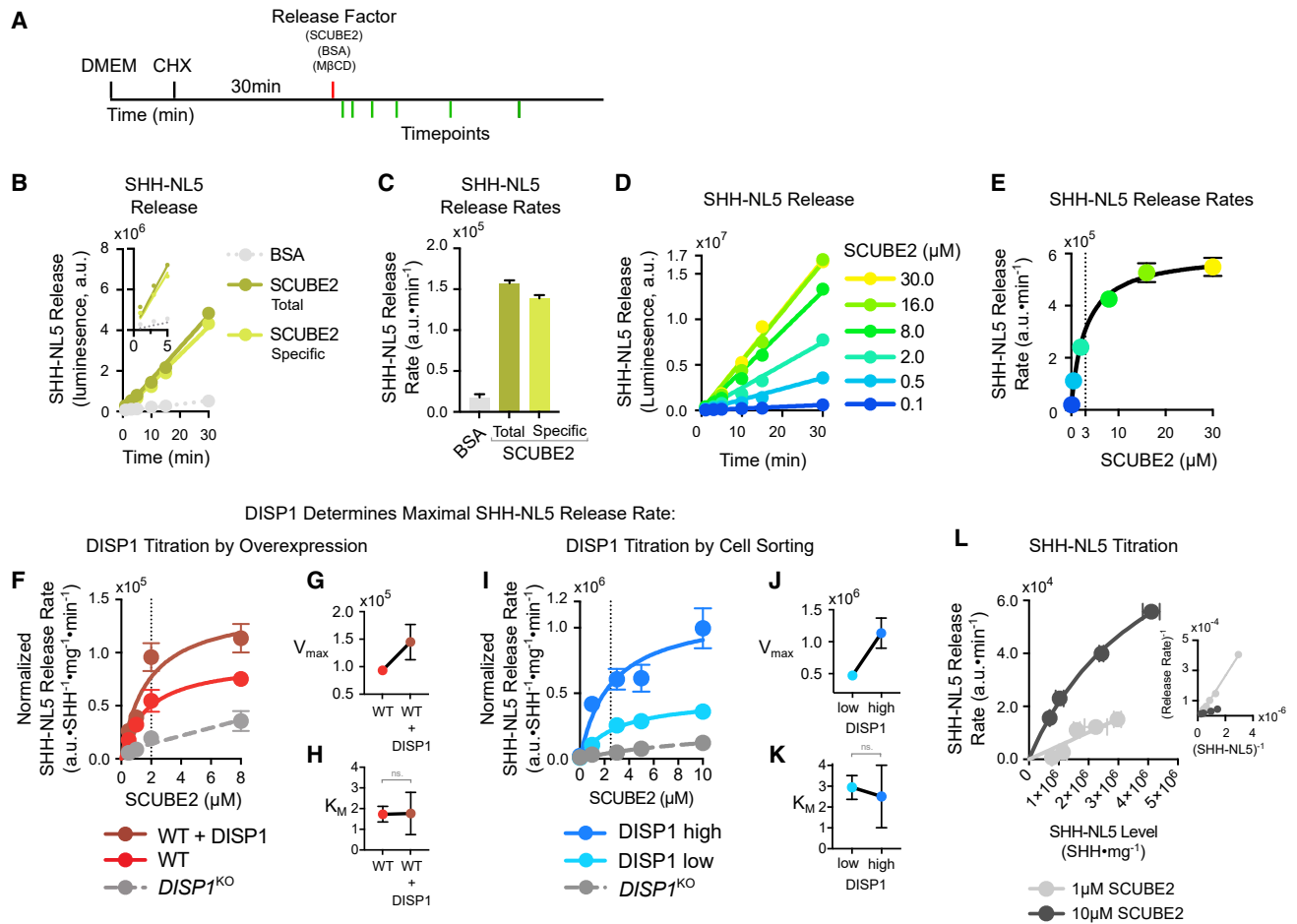
In the experiments above, SHH was collected after several hours and then assayed by immunoblotting. To develop a faster and more sensitive system capable of measuring release kinetics, we tagged SHH with the highly active, ATP-independent NanoLuc luciferase (NL) (Hall et al., 2012), as previously done using *Renilla* luciferase (Ma et al., 2002). The NL tag was introduced internally (Figures S1B and S1C) to preserve SHH modification with palmitate at the N terminus (Chamoun et al., 2001; Pepinsky et al., 1998) and cholesterol at the C terminus (Porter et al., 1996). A total of nine SHH-NL fusions were generated, with different NL insertion sites into SHH (Figures S1B and S1C) (Ma et al., 2002) and were screened for SCUBE2-dependent release from cells. As shown in Figure S1D, the release of three of the SHH-NL fusions was stimulated by SCUBE2 co-expression. The two best-behaved fusions, SHH-NL5 and SHH-NL7, were then tested using purified recombinant SCUBE2 (Figure S1E). As shown in Figure S1F, SHH-NL5 and SHH-NL7 were released in a SCUBE2-dependent manner and could be detected in the culture media by luminescence after much shorter times than SHH detection by immunoblot (Figure 1C). Subsequent experiments were performed using SHH-NL5 (Figure 1D). Significantly, SHH-NL5 was released from cells at similar levels and with the same kinetics as untagged SHH (Figures 1E and S1G–S1I), and luminescence and immunoblot measurements of SHH-NL5 were strongly correlated (Figure S1J). Importantly, SHH-NL5 release from cells requires both DISP1 and SCUBE2 (Figure 1F), indicating its suitability for studying physiological SHH release.

DISP1 Catalyzes SHH Release from Cells

To determine if DISP1 functions as a transporter, we first characterized the kinetics of SHH-NL5 release from cells. To avoid the potentially confounding effect of the continued SHH-NL5 production, protein synthesis was blocked with cycloheximide (Figure 2A). Adding a fixed concentration of purified SCUBE2 caused an increase in SHH-NL5 release that was linear with time (Figures 2B and 2C). Although release by SCUBE2 could be robustly measured after less than 1 min, strictly linear release continued for the entire 30-min duration of the experiment (Figure 2B). Furthermore, the 30-min incubation with SCUBE2 had a negligible effect on cellular SHH-NL5 levels (Figures S2A and S2B), indicating that the SHH-NL5 substrate was saturating under these experimental conditions. Similar DISP1- and SCUBE2-dependent initial release rates were observed for SHH(C24A)-NL5, which is cholesterylated but not palmitoylated, consistent with the idea that the SHH cholesterol moiety serves as a substrate for DISP1 (Figure S2C). Together, these results indicate that our system can be used to precisely measure initial rates of DISP1- and SCUBE2-dependent SHH release (Figure 2C).

Upon titration of purified SCUBE2 added to SHH-NL5-expressing cells, we observed a saturable increase in the initial rate of SHH-NL5 release (Figures 2D and 2E). Importantly, though the rate of release saturated, SHH-NL5 release did not, in line with our finding that cellular SHH-NL5 levels were not limiting (Figures S2A and S2B). This kinetic behavior is not consistent with a simple SHH-SCUBE2 binding equilibrium, where the SHH release rate would be a linear function of SCUBE2; it is consistent, however, with an enzymatic process, whereby formation of the SHH-SCUBE2 complex is catalyzed by a saturable (i.e., rate-limiting) enzyme. Indeed, the rate of SHH-NL5 release is fit well by a simple Michaelis-Menten equation ($R^2 = 0.9954$), with K_M in the low micromolar range of SCUBE2 ($K_M \sim 3 \mu\text{M}$) (Figure 2E; see STAR Methods).

We next asked if DISP1 is the enzyme catalyzing SHH release. To this end, we compared the rate of SCUBE2-dependent SHH-NL5 release from cells expressing different levels of DISP1 (Figures 2F–2K and S2H–S2K). DISP1 was titrated either by expressing additional DISP1 on top of endogenous DISP1 (Figures 2F–2H, S2D, and S2E), by isolating low and high DISP1-expressing cells by fluorescence-activated sorting (Figures 2I–2K, S2F, and S2G), or by expressing DISP1 by transient transfection of *DISP1*^{KO} cells (Figures S2H–S2K). In all cases, the rate of SHH-NL5 release was potentiated by increasing DISP1 levels and was saturable by SCUBE2 (Figures 2F, 2I, and S2H). Crucially, increasing DISP1 levels increased the maximal rate of SHH-NL5 release (V_{max}) (Figures 2G, 2J, and S2I) but not the K_M , which remained 2–3 μM (Figures 2H, 2K, and S2J); this result strongly implies that DISP1 catalyzes SHH release (see STAR Methods). SHH-NL5 release by DISP1 and SCUBE2 is in stark contrast to SHH-NL5 release by methyl- β -cyclodextrin (M β CD), a sterol-binding cyclic oligosaccharide that efficiently solubilizes cholesterylated SHH from membranes (Tukachinsky et al., 2012). SHH-NL5 release by M β CD was DISP1-independent (Figures S2L–S2N), and the rate was a linear function of M β CD concentration, as expected for an uncatalyzed process. Furthermore, SHH-NL5 release by M β CD was more than



DISP1 Determines Maximal SHH-NL5 Release Rate:

DISP1 Titration by Overexpression

DISP1 Titration by Cell Sorting

SHH-NL5 Titration

Figure 2. DISP1 Catalyzes SHH Release from Cells

(A) Schematic of the release assay. Cells stably expressing SHH-NL5 are washed of serum, and protein synthesis is inhibited by pre-incubation with cycloheximide (CHX). SHH-NL5 release is initiated by the addition of purified SCUBE2, and SHH-NL5 in the media is measured at various time points, by NanoLuc luminescence. Bovine serum albumin (BSA) and methyl-β-cyclodextrin (MβCD) serve as controls.

(B) Kinetics of SHH-NL5 release by a fixed concentration of purified SCUBE2 (1 μM). SCUBE2 strongly stimulates SHH-NL5 release, while BSA (1 μM) has no effect. SHH-NL5 release by SCUBE2 is linear over the 30-min duration of the experiment. Inset shows SHH-NL5 release can be robustly detected 1 min after the addition of SCUBE2.

(C) SHH-NL5 initial release rates. Data represent slope estimates in (B) with error bars showing standard error of the estimate.

(D) Time course of SHH-NL5 release by different concentrations of purified SCUBE2.

(E) SHH-NL5 initial release rates from the experiment in (D), plotted as a function of SCUBE2 concentration. Data represent slope estimates and error bars standard error of the estimate. Data were fit to the Michaelis-Menten equation using least-squares, nonlinear regression.

(F) As in (E), but with SHH-NL5 stably expressed in wild-type cells, *DISP1*^{KO} cells, or cells overexpressing wild-type DISP1. Initial release rates were normalized to SHH-NL5 expression levels in each cell line, and to total cell number (total protein) in each experimental condition. SHH-NL5 initial release rates increase with increasing DISP1 levels, while displaying saturation relative to SCUBE2. Curves show fits either to the Michaelis-Menten equation or to a line in the case of *DISP1*^{KO} cells. The vertical dotted line shows K_M estimate. See also [Figures S2D](#) and [S2E](#).

(G) Estimates of V_{max} for the indicated conditions in (F). Error bars indicate the standard error of the estimate.

(H) Estimates of K_M for the indicated conditions in (F). Error bars indicate the standard error of the estimate. ns, not statistically significant

(I) As in (F), but with SHH-NL5- and DISP1-expressing cells sorted into low or high DISP1-expressers. See also [Figures S2F](#) and [S2G](#).

(K) As in (G), but with data from (I).

(J) As in (H), but with data from (I).

(L) SCUBE2-dependent SHH-NL5 release as a function of increasing SHH-NL5 levels. Variable amounts of SHH-NL5 were expressed in cells with endogenous DISP1 and initial release rates recorded for low (1 μM) and high (10 μM) SCUBE2. At high SCUBE2 concentrations, release saturates as a function of SHH-NL5 level, as indicated by good hyperbolic fit (R² = 0.998). Inset shows Lineweaver-Burk plot of the data with accompanying linear fits (R² = 0.996 and R² = 0.995 for low and high SCUBE2, respectively). Data represent rate estimates versus mean SHH-NL5 level. Vertical error bars represent standard error of the estimate; horizontal error bars represent the standard deviation of the mean. See also [Figure S2O](#).

See also [Figure S2](#) for additional characterization of SHH-NL5 release.

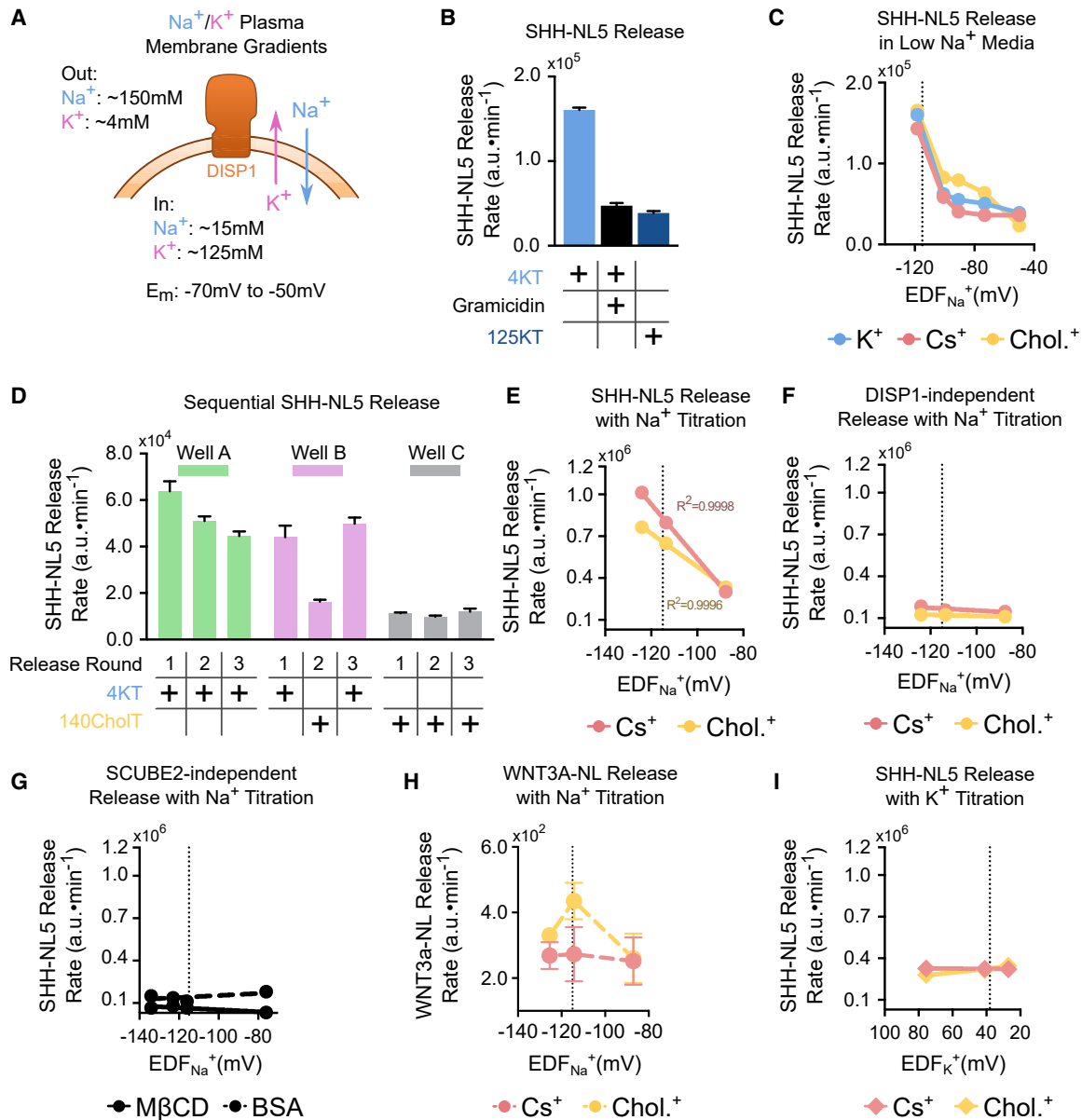


Figure 3. The Na⁺ Gradient Drives DISP1-Catalyzed SHH Release

(A) Schematic of Na⁺ and K⁺ gradients at the plasma membrane in resting mammalian cells.

(B) Cells stably expressing SHH-NL5 were incubated with SCUBE2 (1 μM), in normal Tyrode's media (4KT), 4KT supplemented with gramicidin (2 μg/mL), or media with high K⁺ and low Na⁺ (Tyrode's containing 125 mM KCl, 125KT), and SHH-NL5 release was measured. Protein synthesis was inhibited with CHX (100 μg/mL). Dissipating Na⁺ and K⁺ gradients with gramicidin or 125KT inhibits SHH-NL5 release. Data represent rate estimates with error bars showing the standard error of each estimate.

(C) As in (B), but with incubation in Tyrode's media in which Na⁺ is replaced with K⁺, Cs⁺, or choline⁺. Replacement of extracellular Na⁺ inhibits SHH-NL5 release in a dose-dependent manner, indicating that the Na⁺ gradient is required for DISP1 activity. The electrochemical driving force (EDF) was calculated as described in STAR Methods. Data represent rate estimates; error bars are small and obscured but indicate the standard error of each estimate.

(D) Decreasing extracellular Na⁺ concentration causes rapid and reversible inhibition of SHH-NL5 release. SCUBE2-dependent SHH-NL5 release was measured as in (B), from cells successively incubated in media with physiological Na⁺ (4KT), then with low Na⁺ and high choline⁺ (140CholT), and finally with physiological Na⁺ again (Well B). In parallel, cells were incubated successively only in media with physiological Na⁺ (Well A), or only in media with low extracellular Na⁺ (Well C). Data represent rate estimates with error bars showing the standard error of each estimate.

(E) As in (B), but with incubation in media with varying Na⁺ concentration. Equal osmolarity was maintained with the addition of either Cs⁺ or choline⁺. SHH-NL5 release is accelerated by a steeper than normal Na⁺ gradient. Data represent rate estimates; error bars are small and obscured but indicate the standard error of each estimate. Curves show linear fits with associated R² values. Vertical dotted lines indicate the physiological value of EDF_{Na⁺}.

(F) As in (E), but using SHH-NL5-expressing *DISP1*^{KO} cells. SHH-NL5 release is not accelerated by a steeper Na⁺ gradient in the absence of DISP1.

(G) As in (E), but using MβCD (1 mM) or BSA (5 μM) instead of SCUBE2. SHH-NL5 release is not accelerated by a steeper Na⁺ gradient in the absence of SCUBE2.

(legend continued on next page)

an order of magnitude slower, pointing to the specificity of the DISP1-SCUBE2 system for SHH transport.

Finally, if DISP1 acts as an enzyme to catalyze SCUBE2-dependent SHH release, we would expect the formation of a DISP1-SHH-SCUBE2 ternary complex, which predicts release rate saturation at high concentrations of SCUBE2 and SHH-NL5 (see [STAR Methods](#)). To test this, we titrated SHH-NL5 expression by transient transfection in cells with endogenous DISP1 ([Figure S2O](#)) and measured the rate of SHH-NL5 release at low (1 μ M) and high (10 μ M) SCUBE2 ([Figure 2L](#)). Importantly, at high SCUBE2 concentrations the rate saturated as a function of SHH-NL5. These data are further consistent with DISP1 enzymatic activity and suggest the formation of a ternary DISP1-SHH-SCUBE2 complex. Together, these results indicate that DISP1 catalyzes the release of SHH from cells.

The Transmembrane Na⁺ Gradient Is Necessary for DISP1 Activity

Given the homology between DISP1 and bacterial RND transporters, we asked whether SHH transport by DISP1 is powered by a cation gradient at the plasma membrane. Na⁺ and K⁺ are the two monovalent cations with appreciable concentration gradients across the plasma membrane of metazoan cells; at rest, Na⁺ concentration is high outside the cell and low inside, while K⁺ concentration shows the opposite distribution ([Figure 3A](#)). We first measured SHH-NL5 release in cells treated with gramicidin, a pore-forming antibiotic specific for monovalent cations, which abolishes both Na⁺ and K⁺ gradients. As shown in [Figure 3B](#), the SHH release rate was greatly reduced by gramicidin; importantly, gramicidin did not affect cell viability ([Figure S3A](#)) over the course of the experiment. A similar result was observed when cells were incubated in isotonic media in which Na⁺ was replaced with K⁺ ([Table S1](#)), a treatment that also diminishes both Na⁺ and K⁺ gradients ([Figure 3B](#)). Importantly, the H⁺-specific ionophore carbonyl cyanide 3-chlorophenylhydrazone (CCCP), which equilibrates H⁺ gradients across membranes, had a minimal effect on SHH release ([Figure S3B](#)), thus excluding H⁺ as a potential driver of DISP1 activity. Together, these results suggest that a monovalent, non-H⁺ cation gradient is necessary for SHH release, although they do not identify which ion is involved.

To test the possible role of the Na⁺ gradient, we measured SHH-NL5 release from cells incubated in defined low-Na⁺ media, adjusted to isotonicity with chloride salts of the cations K⁺, Cs⁺, choline⁺, or N-methyl-D-glucamine (NMDG⁺) ([Table S1](#)). In all cases, we observed a dose-dependent decrease in the release rate with decreasing extracellular Na⁺ ([Figures 3C](#), [S3C](#), and [S3D](#)). This effect cannot be attributed to decreases in the membrane potential because Cs⁺, choline⁺, and NMDG⁺ ions are not membrane permeant at short timescales, and thus, do not depolarize the cells, as high extracellular K⁺ does ([Figure S3E](#)). Importantly, the observed effect was not caused by cellular toxicity, as shown by measurements of cellular ATP levels ([Figure S3F](#)) and of NAD(P)H levels ([Figure S3G](#)). Further-

more, inhibition of Na⁺-dependent SHH-NL5 release was rapidly reversible: release rate was greatly reduced upon replacement of extracellular Na⁺ with choline⁺ and then quickly recovered (<1 min) when cells were returned to media with high extracellular Na⁺ ([Figure 3D](#)). Finally, DISP1-independent SHH-NL5 release by M β CD occurred normally in low-Na⁺ media ([Figure S3H](#)), indicating that the SHH-NL5 substrate remains accessible to extracellular factors, on the cell surface. Together, these results indicate that the Na⁺ gradient is required for DISP1-dependent SHH release.

The Na⁺ Gradient Drives SHH Release from Cells

The acute response of SHH release to transient perturbations of the Na⁺ gradient ([Figure 3D](#)) suggests that perhaps Na⁺ directly drives the function of DISP1. One implication of this hypothesis is that the rate of SHH release should be potentiated by a steeper than normal Na⁺ gradient across the plasma membrane. To test this prediction, we measured V_{\max} for SHH release when extracellular Na⁺ concentration was increased above normal. Since the Na⁺ concentration that we tested caused the media to be slightly hypertonic (370 mOsm), all media used in this experiment were adjusted to the same osmolarity using either choline⁺ or Cs⁺ cations instead of Na⁺. V_{\max} was measured by adding saturating levels of purified SCUBE2 (15 μ M, corresponding to \sim 5 times the K_M value). Strikingly, increasing the strength of the Na⁺ gradient accelerated SHH-NL5 release, with the rate displaying a linear ($R^2 > 0.999$) dependence on the Na⁺ electrochemical driving force (EDF_{Na^+}) ([Figure 3E](#)). Significantly, media in which Na⁺ was replaced with choline⁺ did not exhibit changes in membrane potential ([Figure S3I](#)), thus excluding membrane potential change as the cause of the accelerated SHH release. We were unable to detect DISP1- and SCUBE2-dependent uptake of radioactive ²²Na⁺ into cells ([Lee, 1984a, 1984b](#)); perhaps the DISP1 turnover number is too low relative to the background ion fluxes across the plasma membrane.

We performed several experiments to test the specificity of Na⁺ perturbations on DISP1- and SCUBE2-dependent SHH-NL5 release. First, we assayed the effect of Na⁺ gradient change on residual SHH-NL5 release from *DISP1*^{KO} cells ([Figure 3F](#)). Second, we assayed the effect of Na⁺ gradient change on SHH-NL5 release by M β CD, which is SCUBE2-independent ([Figure 3G](#)). Third, we assayed the effect of Na⁺ gradient change on the release of NL-tagged WNT3A, a lipidated Wnt family ligand unrelated to SHH ([Figures 3H](#) and [S3J–S3L](#)). Finally, we assayed the effect of K⁺ gradient change on DISP1- and SCUBE2-dependent SHH-NL5 release, using hypertonic media in which Na⁺ was maintained at physiological levels but extracellular K⁺ was varied ([Figure 3I](#)). In none of these experiments did we observe changes in the release rate of either SHH or WNT3A. Together, these results indicate that the Na⁺ gradient specifically drives DISP1- and SCUBE2-dependent release of SHH, consistent with DISP1 being powered by Na⁺ influx.

(H) As in (E), but with L cells stably expressing WNT3A-NL, and measuring WNT3A-NL release into media containing 2% FBS. WNT3A-NL release is unaffected by changes in the Na⁺ gradient. WNT3A-NL faithfully mimics serum- and palmitoylation-dependent release of untagged WNT3A (see [Figures S2K–S2L](#)).

(I) As in (E), but with incubation in media with varying K⁺ concentration, and constant Na⁺ gradient. The rate of SHH-NL5 release is unaffected by changes in the K⁺ gradient.

See also [Figure S3](#) for additional experiments demonstrating the role of the Na⁺ gradient and for additional controls.

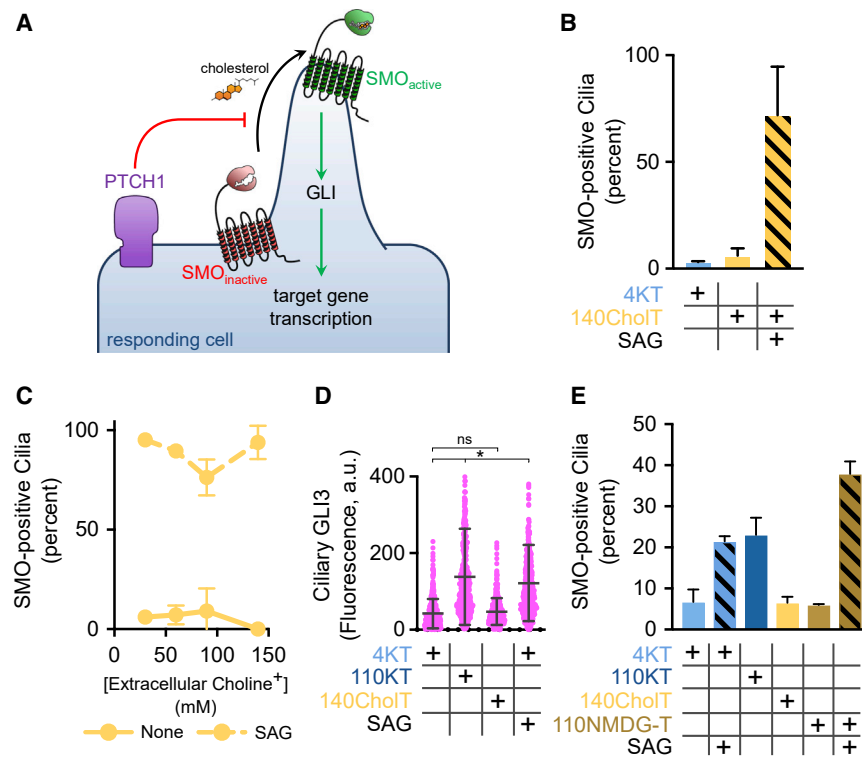


Figure 4. The Na⁺ Gradient Is Dispensable for PTCH1 Function

(A) PTCH1 is required for repressing SMO in Hh-responding cells, by antagonizing SMO activation by cholesterol. It is unknown what powers the essential activity of PTCH1.

(B) Confluent NIH-3T3 cells were serum-starved overnight, to promote ciliogenesis, and were then incubated for 3 h in normal Tyrode's media (4KT) or in media in which Na⁺ was replaced by choline⁺ (140ChoIT). Ciliary levels of endogenous SMO were measured by immunofluorescence microscopy. Staining for the cilium-resident protein ARL13B was used to identify cilia. Abolishing the Na⁺ gradient does not cause SMO ciliary accumulation. The SMO agonist SAG (500 nM) causes ciliary accumulation of SMO in the absence of the Na⁺ gradient. Data show the mean of three biological replicates, and error bars show standard deviation around the mean. At least 100 cilia were recorded per replicate.

(C) As in (B), but varying the concentration of choline⁺ replacing extracellular Na⁺. Varying the Na⁺ gradient does not lead to SMO ciliary accumulation. SMO responds to SAG irrespective of Na⁺ concentration. Data show the mean of three biological replicates, and error bars show standard deviation around the mean. At least 100 cilia were recorded per replicate.

(D) As in (B), but measuring the fluorescence intensity of endogenous GLI proteins in cilia. Low

Na⁺ does not lead to GLI accumulation in cilia, in contrast to SAG or high extracellular K⁺ (110KT, see below). At least 300 cilia per condition were measured in a single biological replicate. *p < 0.05, unpaired, two-tailed t test.

(E) As in (B), but replacing extracellular Na⁺ with NMDG⁺ (110NMDG-T) or K⁺. SMO is not recruited to cilia in 110NMDG-T, in contrast to SAG or 110KT.

The Transmembrane Na⁺ Gradient Is Not Required for PTCH1 Activity

We next asked if and how PTCH1, the other RND-related protein involved in Hh signaling, might also act as a cation-driven transporter, a longstanding hypothesis in the field (Ingham et al., 2000; Taipale et al., 2002). In the absence of SHH, PTCH1 localizes to primary cilia (Rohatgi et al., 2007) and prevents the accumulation of SMO in cilia. Upon binding SHH, PTCH1 is inhibited and removed from cilia. This results in SMO activation and accumulation in cilia (Corbit et al., 2005), leading to ciliary recruitment and activation of GLI-family transcription factors (Humke et al., 2010; Tukachinsky et al., 2010), which ultimately turn on the transcription of Hh target genes, such as *Gli1* (Figure 4A). Since SMO is the most proximal downstream target of PTCH1, and SMO accumulation in cilia is the fastest readout for Hh pathway activation, we used it to measure PTCH1 activity and its sensitivity to cation gradient perturbations. In some instances, we used additional readouts of SMO and Hh pathway activation, namely, ciliary accumulation of GLI proteins and transcription of the Hh target gene, *Gli1*.

SMO and downstream Hh signaling were not activated when the Na⁺ gradient was abolished by incubating cells in media in which Na⁺ was replaced with choline⁺ (Figures 4B–4E), or NMDG⁺ (Figure 4E); this shows that, in the absence of the Na⁺ gradient, SMO is efficiently repressed, thus PTCH1 is active. Importantly, even in the absence of the Na⁺ gradient, cells retained their ability to robustly activate Hh signaling in response to the small-molecule SMO agonist, SAG (Chen et al., 2002) (Fig-

ures 4B–4E). Thus, in contrast to DISP1, the Na⁺ gradient is not required for PTCH1 function.

The Transmembrane K⁺ Gradient Is Necessary for PTCH1 Activity

Dramatically, replacing extracellular Na⁺ with K⁺ or Rb⁺ caused the Hh pathway activation in NIH-3T3 cells, as indicated by ciliary accumulation of SMO (Figures 5A, 5B, and S4A) and GLI proteins (Figures 5C and S4B) and stimulation of *Gli1* transcription (Figure 5D). In all cases, the small-molecule SMO antagonist, SANT-1 (Chen et al., 2002), reversed these effects (Figures 5A, 5C, 5D, and S4B), indicating that Hh pathway activation was SMO-dependent. SMO activation by high extracellular K⁺ was also observed in mouse embryonic fibroblasts (MEFs) (Figure S4C). Together, these results suggest that the K⁺ gradient might be required for PTCH1 function.

We also tested whether reducing the K⁺ gradient inhibits PTCH1 reversibly. Hh signaling was activated with SHH, which caused the accumulation of SMO in cilia (Figure 5E). SHH was then washed out, and we measured the decay of ciliary SMO, a process dependent on PTCH1 activity. As shown in Figure 5E, ciliary SMO was removed from cilia in media of normal ionic composition but not in high K⁺ media. Importantly, PTCH1 activity was recovered when cells were switched from high to low K⁺, indicating that the inhibitory effect is reversible.

The treatments above alter not only the K⁺ gradient but also have other effects on cells, including possible perturbations of ciliary trafficking, energy metabolism, Ca²⁺ levels, and resting

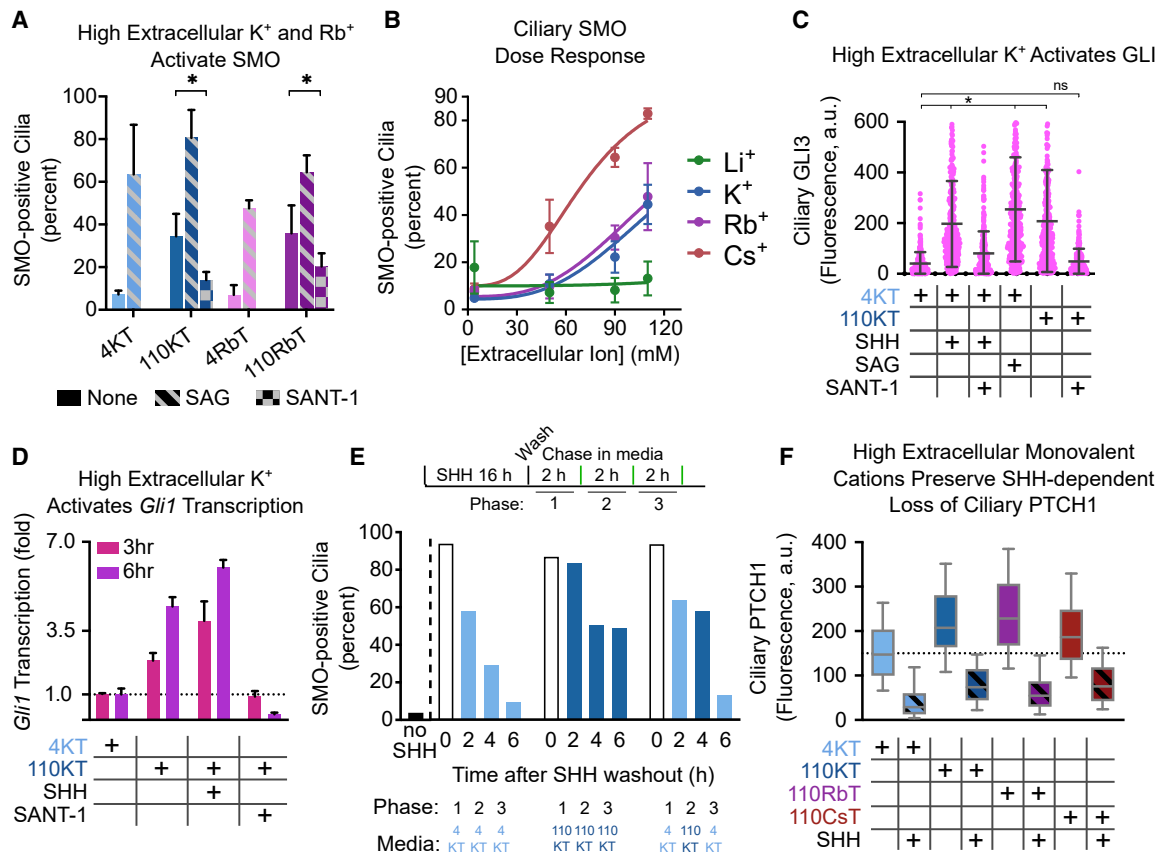


Figure 5. The K⁺ Gradient Is Necessary for PTCH1 Function

(A) Ciliated NIH-3T3 cells were incubated for 3 h in media with either low (4KT, 4RbT) or high (110KT, 110RbT) K⁺ or Rb⁺, and endogenous SMO at cilia was measured by immunofluorescence. High K⁺ or Rb⁺ leads to SMO accumulation in cilia, which is reversed by the SMO antagonist, SANT-1 (1 μM). SAG (500 nM) was used as a positive control. Data represent mean of at least two biological replicates; error bars show standard deviation around the mean. At least 100 cilia were assayed per replicate. *p < 0.05, unpaired, two-tailed t test.

(B) As in (A), but with incubation in isotonic media in which Na⁺ is replaced with various concentrations of monovalent cations (Li⁺, K⁺, Rb⁺, Cs⁺). Hill equation curves with Hill slope of 3 and maximum value of 100% were fit to the data. Data represent mean of at two biological replicates; error bars show standard deviation around the mean. At least 100 cilia were assayed per replicate.

(C) As in (A), but measuring endogenous GLI proteins in cilia. GLI proteins are recruited to cilia in media with high extracellular K⁺ (110KT), which is reversed by SANT-1. The Hh pathway activators SHH and SAG were used as positive controls. At least 250 cilia were assayed per treatment condition in a single biological replicate. *p < 0.001, one-way ANOVA.

(D) As in (A), but measuring transcription of *Gli1* by quantitative RT-PCR, after incubation for 3 and 6 h. *Gli1* transcription is activated in 110-KT media, which is reversed by SANT-1. SHH was used as positive control.

(E) Reducing the K⁺ gradient causes reversible inhibition of PTCH1. NIH-3T3 cells were stimulated overnight with SHH, after which they were chased in media of varying K⁺ concentration, and ciliary SMO was measured at different times. Ciliary SMO levels drop quickly in 4KT media, but persist in 110KT, in which PTCH1 is inactive. Switching cells from 4KT to 110KT inhibits PTCH1 and thus SMO removal from cilia, which is reactivated by switching back to 4KT media. At least 250 cilia were assayed per condition in a single biological replicate.

(F) Ciliated NIH-3T3 cells stably expressing EGFP-tagged PTCH1 were incubated for 3 h in the indicated media, in the presence or absence of SHH, and PTCH1 levels in cilia were measured by immunofluorescence. High levels of extracellular K⁺, Rb⁺, or Cs⁺ do not perturb SHH-induced removal of PTCH1 from cilia. PTCH1 fluorescence intensity at cilia is shown as box-and-whisker plots for a single biological replicate. The dotted line shows the threshold used to compute the percent PTCH1-positive cilia (Figure S4D). At least 100 cilia were assayed per condition.

See also Figure S4 for additional experiments demonstrating the role of the K⁺ gradient in Hh signaling

membrane potential (E_m). To exclude the possibility that one of these perturbations might have caused SMO activation, we performed a number of control experiments. First, we assayed the effect of high extracellular K⁺ or Rb⁺ on ciliary trafficking, by measuring PTCH1 removal from cilia upon SHH binding, as well as by assaying the constitutive ciliary localization of serotonin receptor 6 (HTR6). High K⁺ or Rb⁺ allowed normal SHH-induced PTCH1 exit from cilia (Figures 5F and S4D), while high

K⁺ did not change ciliary HTR6 levels (Figure S4E). These results indicate that high extracellular K⁺ or Rb⁺ do not generally perturb ciliary trafficking.

Second, we measured cellular ATP levels in cells incubated with high extracellular K⁺ or Rb⁺. We found that high extracellular K⁺ or Rb⁺ reduced cellular ATP by 40%–50% compared with low extracellular K⁺ (Figure S3F). We speculated that reduction in cellular ATP may be responsible for the blunted pathway

activation that we observed with these treatments; however, it is not sufficient to explain the observed pathway activation.

Third, we investigated whether divalent cations, Ca^{2+} and Mg^{2+} , affect SMO ciliary dynamics and whether they are required for SMO activation in the presence of high extracellular K^+ or Rb^+ . By incubating cells in media lacking extracellular Ca^{2+} and Mg^{2+} , we observed that extracellular pools of Ca^{2+} and Mg^{2+} are dispensable for SMO inhibition by PTCH1, for SMO activation in response to SHH, as well as for SMO activation by high levels of extracellular K^+ and Rb^+ (Figure S4F). These data suggest that any putative Ca^{2+} and Mg^{2+} fluxes are not necessary for SMO inhibition by PTCH1.

Fourth, we asked if the membrane depolarization caused by high extracellular K^+ or Rb^+ (Figure S3E), rather than a decrease in K^+ gradient, is the cause of SMO activation. Treating cells with the sodium channel agonist veratridine, which depolarizes cells without collapsing the K^+ gradient (Figure S4G), led only to a very slight increase in ciliary SMO (Figure S4H); thus, cellular depolarization cannot account for SMO activation by high K^+ and Rb^+ .

Finally, we discovered that Cs^+ causes dose-dependent accumulation of SMO in cilia (Figures 5B, S4A, and S4I), which was reversed by SANT-1 (Figure S4I). Cs^+ was also more potent than K^+ or Rb^+ in activating SMO (Figures 5B and S4I). Cs^+ did not perturb PTCH1 ciliary trafficking (Figures 5F and S4D), cellular ATP levels (Figure S3F), and did not depolarize cells (Figure S3E), consistent with a specific inhibitory effect on PTCH1. Interestingly, Cs^+ did not collapse the K^+ gradient, suggesting a different explanation for its effect. We note that the potency of PTCH1 inhibition increases as a function of van der Waals radius for K^+ , Rb^+ , and Cs^+ (Figure S4J); we speculate that Cs^+ , and to a lesser extent Rb^+ , might inhibit PTCH1 by occluding a putative cation-conducting pore in PTCH1.

A Possible Mechanism for Cation-Dependent DISP1 and PTCH1 Function

We used structure-guided mutagenesis and functional assays to probe the role of cations in DISP1 and PTCH1 function. Homology between DISP1, PTCH1, and H^+ -powered bacterial RNDs is highest within their transmembrane (TM) domains. In particular, there is striking conservation of three sets of polar residues within helices TM4, TM10, and TM11 (Figure 6A). In AcrB (Murakami et al., 2006; Seeger et al., 2006), these residues form an alternating hydrogen-bonding network (Figure 6B). In the absence of protons, the two neighboring aspartate residues in TM4 (D407 and D408) are ionized and coordinate the ϵ -amino group of the lysine residue in TM10 (K940). In the presence of protons, the glutamic acid residues in TM4 are titrated, and the ϵ -amino group of the lysine in TM10 now interacts with the serine and threonine residues in the neighboring TM11 (T978 and S979). By altering the hydrogen-bonding network of these TM-resident residues, AcrB couples proton binding to conformational changes that enable substrate pumping (Pos, 2009). Consistent with this mechanism, the three sets of polar residues are necessary for AcrB function (Su et al., 2006; Takatsuka and Nikaido, 2006).

While DISP1 and PTCH1 both contain the TM4-resident aspartate found in bacterial RNDs, they lack the opposing, TM10-resident lysine; instead, this residue is replaced with an acidic one, either aspartate in DISP1 or glutamate in PTCH1 (Figure 6A). We

hypothesize that the triad of acidic residues in TM4 and TM10 of DISP1 and PTCH1 forms a cation-binding pocket, such that, in the cation's presence, a salt bridge forms between TM4 and TM10, analogous to the link between TM4 and TM10 in unprotonated AcrB (Figure 6C). Upon cation dissociation, the negative charge of these residues would lead to electrostatic repulsion and dissolution of the salt bridge, and formation of a hydrogen bond between the first TM4 aspartate of DISP1 and PTCH1 and the TM11 serine/threonine cluster (Figure 6C). At least for PTCH1, evidence of such an alternating hydrogen-bonding network can be found in recent cryo-EM structures (Figure S5).

The prediction of this model is that this set of polar residues would be necessary for DISP1 and PTCH1 function. This was shown for the TM4 aspartate residues in both DISP1 (Ma et al., 2002) and PTCH1 (Taipale et al., 2002). Additionally, we found that the TM11 serine/threonine cluster is absolutely required for DISP1 (Figures 6D, S6A, and S6B) and PTCH1 (Figures 6E and S6C) function. In accordance with the proposed mechanism (Figure 6C), the introduction of a lysine residue (i.e., non-dissociating cation) within the TM4-TM10-TM11 network drastically inhibits both DISP1 (Figures 6D, S6A, and S6B) and PTCH1 (Figures 6E and S6C). Finally, we found that low pH inhibits, while high pH potentiates DISP1 activity (Figure 6F), an effect that can be explained by protonation of TM-resident acidic residues inhibiting cation coordination. The observed pH dependence is consistent with the calculated pK_a values (Kilambi and Gray, 2012) of the three TM-resident acidic residues in DISP1 (3.8, 3.5, and 4.1, for D571, D572, and D1049, respectively). A similar effect has been observed for the Na^+ -powered human choline symporter (hCHT) (Iwamoto et al., 2006). Together, these data support DISP1 and PTCH1 as transporters powered by non- H^+ cations and point to a possible mechanism for how cation-induced conformational changes in the TM domain are translated into substrate pumping.

DISCUSSION

Among signaling pathways that orchestrate animal embryogenesis, the Hh pathway stands out for the critical role played by cholesterol at two different steps. First, cholesterol is covalently attached to SHH, a unique modification catalyzed by the C-terminal domain of the SHH precursor (Porter et al., 1996). Second, the GPCR-like protein SMO, which conveys signals to the cytoplasm, is directly activated by cholesterol (Huang et al., 2016; Luchetti et al., 2016). In both instances, the pathway employs RND-related proteins: DISP1 interacts with cholesterolated SHH and hands it off to an extracellular SCUBE family protein (Creanga et al., 2012; Tukachinsky et al., 2012), resulting in SHH morphogen release, while PTCH1 interacts with cholesterol and antagonizes SMO, thus repressing Hh signal transduction. Two important open questions are whether eukaryotic RND-like proteins, such as DISP1 and PTCH1, function as transporters, and what is the energy source that powers them. Prokaryotic RNDs use the H^+ gradient across the plasma membrane (Figure 7A), which does not exist in most eukaryotic cells. Here, we directly demonstrated the transporter activity for a eukaryotic RND-like protein, DISP1. We then showed that DISP1 is powered by the Na^+ gradient at the plasma membrane, while the K^+ gradient is dispensable (Figure 7B). Interestingly, we found

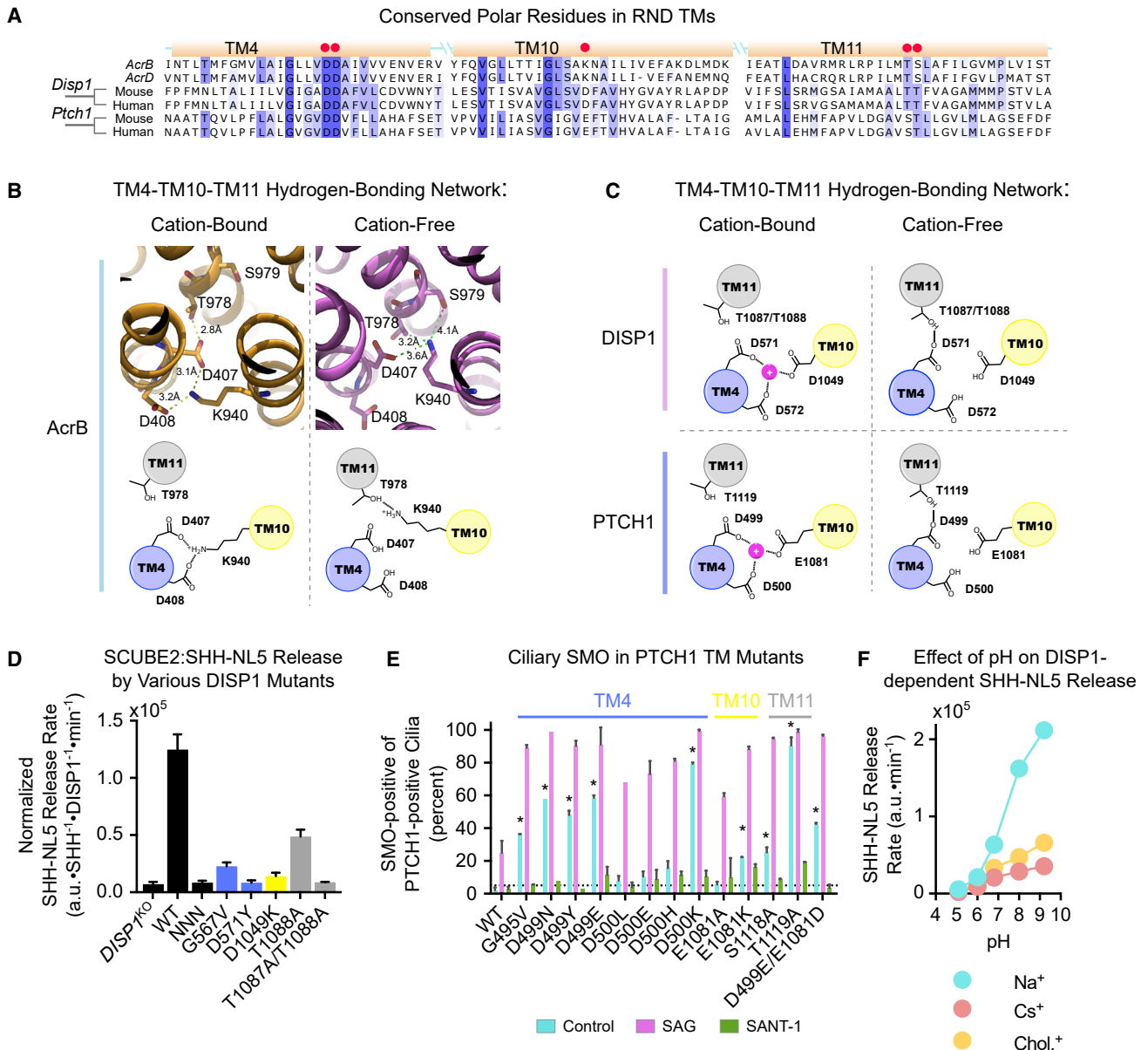


Figure 6. A Conserved Cation-Sensitive Network Necessary for DISP1 and PTCH1 Function

(A) Sequence alignment of DISP1, PTCH1, and *E. coli* AcrB and AcrD. TM helices are shown as yellow boxes, with red dots indicating polar residues necessary for DISP1, PTCH1, and AcrB function.

(B) Proton-dependent conformational changes in AcrB (PDB: 2gjf). TM4-resident D407 and D408 residues alternate between being deprotonated and bound to the TM10-resident K940 (left) and being protonated and with K940 bound to T978/S979 in TM11 (right).

(C) Proposed model of cation-dependent conformational switching in DISP1 and PTCH1. TM10 hosts an aspartate in DISP1 and glutamate in PTCH1, instead of a lysine. This suggests that the deprotonated acidic residues in TM4 and TM10 form a cation-binding site. In the absence of cation, the first TM4 aspartate binds to the S/T cluster in TM11, to effect conformational change. Residue numbers are for mouse DISP1 and PTCH1.

(D) TM-resident polar residues in DISP1 are necessary for SHH release. *DISP1*^{KO} HEK293T cells stably expressing SHH-NL5 were stably rescued with DISP1 mutants, and SCUBE2-dependent SHH-NL5 release was measured. Protein synthesis was inhibited with CHX (100 μg/mL). Data show an estimate of release rate normalized to DISP1 and SHH-NL5 levels in single biological replicate; error bars represent combined standard error and standard deviation around the mean.

(E) TM-resident polar residues in PTCH1 are necessary for SMO repression. PTCH1 mutants were stably expressed in *Ptch1*^{-/-} MEFs, and their ability to reduce ciliary levels of endogenous SMO was assayed by immunofluorescence. SAG (500 nM) and SANT-1 (1 μM) served as a positive and negative control, respectively. Error bars represent the standard deviation around the mean of two biological replicates. At least 100 cilia were assayed per replicate. **p* < 0.01, unpaired, two-tailed t test.

(F) As in (D), but HEK293T cells stably expressing SHH-NL5 were incubated with SCUBE2 (1 μM), in modified Tyrode's media with high Na⁺, choline⁺ or Cs⁺, buffered to different pH values. SHH-NL5 release is potentiated by increasing pH, but only if the Na⁺ gradient is present. Error bars are obscured but indicate standard error of the estimate in a single replicate.

See also Figure S5 for evidence of an alternating hydrogen-bonding network in PTCH1, similar to AcrB. See also Figure S6 for characterization of cells used for DISP1 and PTCH1 mutant analysis.

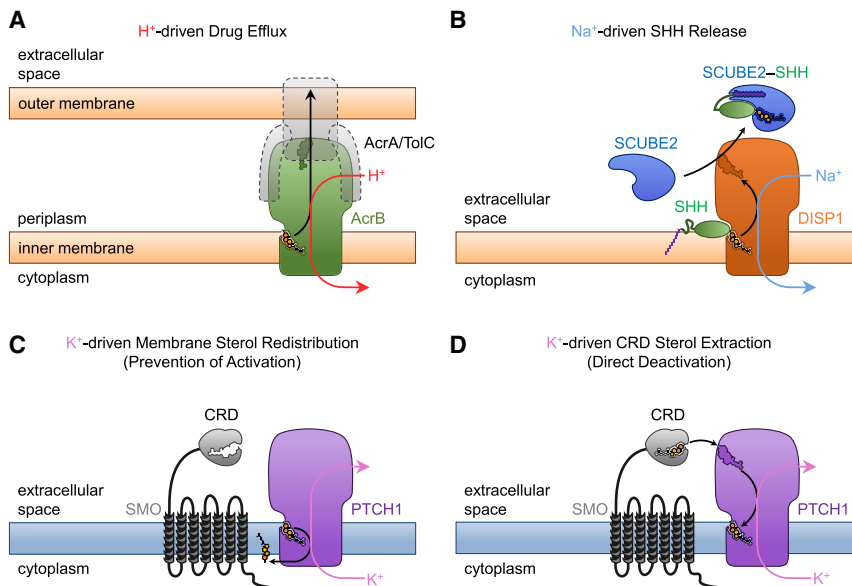


Figure 7. RND-Catalyzed Cholesterol Transport in the Hh Pathway

(A) Schematic of the prototypical prokaryotic H^+ -powered RND transporter, *E. coli* AcrB.

(B) DISP1 functions as a Na^+ -powered antiporter, transporting cholesterylated SHH from the outer leaflet of the plasma membrane and handing it off to extracellular SCUBE2.

(C and D) Two possible modes of K^+ -powered cholesterol transport by PTCH1. In (C), PTCH1 moves cholesterol between the two leaflets of the membrane, making it unavailable for SMO activation. In (D), PTCH1 transports cholesterol from SMO to the membrane, thus catalyzing SMO deactivation.

that PTCH1 displays the opposite behavior: The K^+ gradient is necessary for its activity in Hh signaling, but the Na^+ gradient is dispensable (Figures 7C and 7D). Thus, Na^+ and K^+ , the two monovalent cations that form substantial gradients across the plasma membrane of animal cells, are used to power DISP1 and PTCH1, respectively. Despite diverged cation specificity, however, the mechanism by which cation binding is translated into substrate pumping appears conserved between DISP1, PTCH1, and prokaryotic RNDs, as indicated by our functional studies.

Past investigations of DISP1 (Creanga et al., 2012; Tukachinsky et al., 2012) lacked the sensitivity and temporal resolution needed to address the role of ion gradients. We, therefore, developed a fast and sensitive NL luciferase assay, inspired by an earlier *Renilla* luciferase assay (Ma et al., 2002), which allowed us to directly study the kinetics of SHH substrate release by DISP1 and purified SCUBE2, in media of defined ionic composition. Our measurements indicate that DISP1 is a transporter quantitatively described by Michaelis-Menten kinetics, with a catalytic rate constant (k_{cat}) that is a function of the transmembrane Na^+ gradient. Strikingly, a steeper Na^+ gradient increases k_{cat} and accelerates SHH release, indicating that the Na^+ gradient directly controls DISP1.

Why would DISP1 need energy to catalyze SHH release, given that SHH is likely more concentrated on the membrane than in the extracellular space? We speculate that the cholesteryl anchor of SHH is strongly attached to membrane lipids, resulting in high activation energy for direct SHH transfer to SCUBE2. To catalyze SHH transfer, DISP1 would not only need to provide a pathway for the cholesteryl anchor from the membrane to SCUBE2 but also to overcome the binding energy between anchor and membrane. Importantly, energy consumption would ensure that SHH transfer by DISP1 is unidirectional. Similar considerations apply for energy utilization during cholesterol transport by PTCH1 (see below).

The present kinetic data and previous cross-linking experiments using SHH modified with photoreactive cholesterol ana-

logs (Tukachinsky et al., 2012), are consistent with the formation of a DISP1-SHH-SCUBE2 complex. SHH transfer from DISP1 to SCUBE2 resembles, in reverse, the transfer of cholesterol between the soluble NPC2 protein and

NPC1 (Infante et al., 2008), for which a stable NPC1-NPC2 interaction has been observed (Deffieu and Pfeffer, 2011). We have so far been unable to detect DISP1-SCUBE2 binding, even in the presence of SHH, possibly because such an interaction is transient. Further studies will be necessary to dissect SHH transfer from DISP1 to SCUBE2, and to capture and structurally characterize a possible ternary complex.

Unlike DISP1, the mode and direction of cholesterol transport by PTCH1 are unclear (see below). Thus, instead of directly assaying substrate transport by PTCH1, we measured PTCH1 activity using endogenous downstream readouts of the Hh pathway, primarily the activity state of SMO. We found that PTCH1 represses SMO efficiently and keeps the Hh pathway off even when the Na^+ gradient is abolished, in contrast to DISP1. Strikingly, abolishing the K^+ gradient leads to PTCH1 inhibition and Hh pathway activation, as assayed by SMO and GLI recruitment to primary cilia, and activation of target gene transcription. Importantly, other effects can be excluded as the cause of the Hh pathway activation, including membrane depolarization, energy metabolism, or effects on ciliary trafficking. These results indicate that the K^+ gradient powers PTCH1 activity.

Our observation that the Na^+ gradient is dispensable for SMO repression by PTCH1 contrasts with a recent report claiming that PTCH1 activity requires the Na^+ gradient (Myers et al., 2017). Although the reason for this discrepancy is not clear, it might be due to one of several differences in experimental design. We used MEFs that display robust cilia-dependent Hh signaling, while the other study used HEK293T cells, which lack endogenous Hh signaling. We assayed endogenous SMO, while the other study assayed truncated SMO fused to $G\alpha_i$, a construct of unclear physiological relevance in Hh signaling. Finally, we used physiological readouts of SMO activation, while the other study measured the reduction of forskolin-enhanced cAMP levels.

Our results clarify the relationship between the direction of substrate transport and ion flow in eukaryotic RND-related proteins. In the case of DISP1, cholesterylated SHH is transported from the membrane to the extracellular space, while Na^+ ions

flow along their concentration gradient from the extracellular space inward. Thus, DISP1 is a Na⁺/SHH antiporter, similar to bacterial RNDs, which are H⁺/substrate antiporters, pumping substrates out of the cell while H⁺ ions flow inward.

In the case of PTCH1, the pathway of cholesterol transport remains unresolved, a question with important implications for the mechanism of SMO repression. One suggestion is that PTCH1 moves cholesterol from the inner to the outer leaflet of the plasma membrane (Zhang et al., 2018); however, the imaging method for measuring cholesterol used in this study has been questioned due to its strong dependence on the phospholipid composition of the membrane (Courtney et al., 2018). If PTCH1 is an antiporter, the fact that it is powered by the K⁺ gradient implies that it must transport cholesterol toward the cell, while K⁺ ions flow outward; this is similar to how cholesterol movement occurs in the NPC2-NPC1 system, from the lysosomal lumen into the limiting membrane. For a PTCH1 K⁺/cholesterol antiporter, we envision two possibilities: PTCH1 moves cholesterol from the outer to the inner leaflet of the membrane (Figure 7C), or PTCH1 accepts cholesterol directly from SMO, perhaps from the CRD, and transports it to the outer leaflet of the membrane (Figure 7D). The former model implies that PTCH1 prevents SMO activation by cholesterol, for example, by lowering cholesterol concentration in the ciliary membrane. In contrast, the latter model implies that PTCH1 catalyzes the deactivation of cholesterol-bound SMO. We note that cholesterol transport postulated by this latter model is consistent with recent cryo-EM studies (Gong et al., 2018; Qian et al., 2019), in which sterol densities are observed both in the extracellular domain and in an outer leaflet-proximal groove of PTCH1, suggesting a conduit from SMO to the membrane. An attractive aspect of this model is that it explains the specificity of PTCH1 for SMO and the Hh pathway, in contrast to a model in which PTCH1 transports cholesterol independent of SMO. Another implication of this model is that SMO can bind cholesterol early in the secretory pathway, and PTCH1 would remove it only when SMO reaches the cilium. Importantly, even though cholesterol-bound SMO might adopt an active conformation outside the cilium, it would not trigger Hh signaling, as that requires the presence of cilia-localized pathway components. Functional experiments will be required to elucidate this important aspect of the PTCH1-SMO interaction.

A useful estimate is that of the free energy that transmembrane Na⁺ and K⁺ gradients can provide for cholesterol transport by DISP1 and PTCH1, respectively. The power of an ionic gradient is expressed as Gibbs free energy, which can be calculated according to Equation 1:

$$\Delta G_{\text{ion}} = zF(\text{EDF}_{\text{ion}}) \quad (\text{Equation 1})$$

where, z is the ion charge, F is the Faraday constant, and EDF_{ion} is the electrochemical driving force. In a typical fibroblast ($E_m = -54$ mV, $[\text{Na}^+]_{\text{out}} = 150$ mM and $[\text{Na}^+]_{\text{in}} = 15$ mM) the Na⁺ gradient has an $\text{EDF}_{\text{Na}^+} = -115$ mV, which translates into ~ 11 kJ/mol of free energy available for Na⁺-powered transport by DISP1. In the case of PTCH1, we must consider that it functions at the ciliary membrane (Rohatgi et al., 2007), which has electrophysiological properties slightly different from the plasma membrane (Delling et al., 2013); specifically, at the primary cilium, $E_m = -20$ mV, $[\text{K}^+]_{\text{out}} = 4$ mM and $[\text{K}^+]_{\text{in}} = 70$ mM. These pa-

rameters yield an $\text{EDF}_{\text{K}^+} = 54$ mV, corresponding to ~ 5.2 kJ/mol of free energy available for K⁺-powered cholesterol transport by PTCH1. To put these free energy values in perspective, we consider the Na⁺-powered glucose symporter SGLT2 (Coady et al., 2017) and the Na⁺-powered choline symporter hCHT (Iwamoto et al., 2006). These proteins transport one Na⁺ ion per substrate molecule, and voltage-current studies show that an $\text{EDF}_{\text{Na}^+} > 5$ kJ/mol Na⁺ is sufficient to power these transporters. Thus, the energy supplied by the plasma membrane Na⁺ gradient or by the ciliary K⁺ gradient is likely sufficient to power substrate transport by DISP1 and PTCH1, respectively.

STAR★METHODS

Detailed methods are provided in the online version of this paper and include the following:

- KEY RESOURCES TABLE
- RESOURCE AVAILABILITY
 - Lead Contact
 - Materials Availability
 - Data and Code Availability
- EXPERIMENTAL MODEL AND SUBJECT DETAILS
 - Cell Culture
 - Generation of *DISP1* Knockout (*DISP1*^{KO}) HEK293T Cells by CRISPR/Cas9
- METHOD DETAILS
 - Antibodies
 - DNA Constructs
 - Custom Media Formulations
 - Fluorescence-Activated Cell Sorting
 - Protein Expression and Purification
 - Luciferase-based SHH Release Assays
 - WNT3A Release Assays
 - Total Protein Measurements
 - Immunoblot-based SHH Release
 - Microscopy and Immunofluorescence
 - Quantitative RT-PCR
 - E_m Measurements
 - Cellular ATP Measurements
 - Cellular NAD(P)H Measurements
 - Kinetic Model for DISP1-catalyzed SHH Release
 - Kinetic Model for DISP1 Playing an Accessory Role in SHH Release
 - Calculations of the Electrochemical Driving Force (EDF)
 - Blot Image Processing
- QUANTIFICATION AND STATISTICAL ANALYSIS

SUPPLEMENTAL INFORMATION

Supplemental Information can be found online at <https://doi.org/10.1016/j.devcel.2020.08.002>.

ACKNOWLEDGMENTS

This work was supported by NIH grants R01 GM122920 and GM135262 (to A.S.) and by NIH predoctoral fellowship F31GM120833 (to B.M.W.). We thank Marie Bao for reading the manuscript and for helpful suggestions, and members of the Saïc lab for discussions.

AUTHOR CONTRIBUTIONS

K.P., B.M.W., and A.S. conceived the project and designed and performed the experiments. J.L. conceived and performed WNT3A experiments. K.P. and B.M.W. analyzed data and assembled the figures. K.P., B.M.W., and A.S. wrote the manuscript.

DECLARATION OF INTERESTS

The authors declare no competing interests.

Received: October 4, 2019

Revised: May 7, 2020

Accepted: July 30, 2020

Published: August 28, 2020

REFERENCES

- Aires, J.R., and Nikaido, H. (2005). Aminoglycosides are captured from both periplasm and cytoplasm by the AcrD multidrug efflux transporter of *Escherichia coli*. *J. Bacteriol.* *187*, 1923–1929.
- Alcedo, J., Ayzenzon, M., Von Ohlen, T., Noll, M., and Hooper, J.E. (1996). The *Drosophila* smoothed gene encodes a seven-pass membrane protein, a putative receptor for the hedgehog signal. *Cell* *86*, 221–232.
- Amanai, K., and Jiang, J. (2001). Distinct roles of Central missing and Dispatched in sending the Hedgehog signal. *Development* *128*, 5119–5127.
- Blose, S.H., Meltzer, D.I., and Feramisco, J.R. (1984). 10-nm filaments are induced to collapse in living cells microinjected with monoclonal and polyclonal antibodies against tubulin. *J. Cell Biol.* *98*, 847–858.
- Burke, R., Nellen, D., Bellotto, M., Hafen, E., Senti, K.A., Dickson, B.J., and Basler, K. (1999). Dispatched, a novel sterol-sensing domain protein dedicated to the release of cholesterol-modified hedgehog from signaling cells. *Cell* *99*, 803–815.
- Byrne, E.F.X., Sircar, R., Miller, P.S., Hedger, G., Luchetti, G., Nachtergaele, S., Tully, M.D., Mydock-McGrane, L., Covey, D.F., Rambo, R.P., et al. (2016). Structural basis of smoothed regulation by its extracellular domains. *Nature* *535*, 517–522.
- Carstea, E.D., Morris, J.A., Coleman, K.G., Loftus, S.K., Zhang, D., Cummings, C., Gu, J., Rosenfeld, M.A., Pavan, W.J., Krizman, D.B., et al. (1997). Niemann-Pick C1 disease gene: homology to mediators of cholesterol homeostasis. *Science* *277*, 228–231.
- Caspary, T., García-García, M.J., Huangfu, D., Eggenschwiler, J.T., Wyler, M.R., Rakeman, A.S., Alcorn, H.L., and Anderson, K.V. (2002). Mouse Dispatched homolog1 is required for long-range, but not juxtacrine, Hh signaling. *Curr. Biol.* *12*, 1628–1632.
- Chamoun, Z., Mann, R.K., Nellen, D., von Kessler, D.P., Bellotto, M., Beachy, P.A., and Basler, K. (2001). Skinny hedgehog, an acyltransferase required for palmitoylation and activity of the hedgehog signal. *Science* *293*, 2080–2084.
- Chang, D.T., López, A., von Kessler, D.P., Chiang, C., Simandl, B.K., Zhao, R., Seldin, M.F., Fallon, J.F., and Beachy, P.A. (1994). Products, genetic linkage and limb patterning activity of a murine hedgehog gene. *Development* *120*, 3339–3353.
- Chen, J.K., Taipale, J., Young, K.E., Maiti, T., and Beachy, P.A. (2002). Small molecule modulation of smoothed activity. *Proc. Natl. Acad. Sci. USA* *99*, 14071–14076.
- Coady, M.J., Wallendorff, B., and Lapointe, J.Y. (2017). Characterization of the transport activity of SGLT2/MAP17, the renal low-affinity Na⁺-glucose cotransporter. *Am. J. Physiol. Ren. Physiol.* *313*, F467–F474.
- Cong, L., Ran, F.A., Cox, D., Lin, S., Barretto, R., Habib, N., Hsu, P.D., Wu, X., Jiang, W., Marraffini, L.A., et al. (2013). Multiplex genome engineering using CRISPR/Cas systems. *Science* *339*, 819–823.
- Cooper, M.K., Wassif, C.A., Krakowiak, P.A., Taipale, J., Gong, R., Kelley, R.I., Porter, F.D., and Beachy, P.A. (2003). A defective response to Hedgehog signaling in disorders of cholesterol biosynthesis. *Nat. Genet.* *33*, 508–513.
- Corbit, K.C., Aanstad, P., Singla, V., Norman, A.R., Stainier, D.Y., and Reiter, J.F. (2005). Vertebrate smoothed functions at the primary cilium. *Nature* *437*, 1018–1021.
- Courtney, K.C., Fung, K.Y., Maxfield, F.R., Fair, G.D., and Zha, X. (2018). Comment on "Orthogonal lipid sensors identify transbilayer asymmetry of plasma membrane cholesterol. *eLife* *7*.
- Creanga, A., Glenn, T.D., Mann, R.K., Saunders, A.M., Talbot, W.S., and Beachy, P.A. (2012). Scube/You activity mediates release of dually lipid-modified Hedgehog signal in soluble form. *Genes Dev.* *26*, 1312–1325.
- Davis, H.R., Jr., Zhu, L.J., Hoos, L.M., Tetzloff, G., Maguire, M., Liu, J., Yao, X., Iyer, S.P., Lam, M.H., Lund, E.G., et al. (2004). Niemann-Pick C1 Like 1 (NPC1L1) is the intestinal phytosterol and cholesterol transporter and a key modulator of whole-body cholesterol homeostasis. *J. Biol. Chem.* *279*, 33586–33592.
- Deffieu, M.S., and Pfeffer, S.R. (2011). Niemann-Pick type C 1 function requires luminal domain residues that mediate cholesterol-dependent NPC2 binding. *Proc. Natl. Acad. Sci. USA* *108*, 18932–18936.
- Delling, M., DeCaen, P.G., Doerner, J.F., Febvay, S., and Clapham, D.E. (2013). Primary cilia are specialized calcium signalling organelles. *Nature* *504*, 311–314.
- Delmar, J.A., Su, C.C., and Yu, E.W. (2015). Heavy metal transport by the CusCFBA efflux system. *Protein Sci.* *24*, 1720–1736.
- Echelard, Y., Epstein, D.J., St-Jacques, B., Shen, L., Mohler, J., McMahon, J.A., and McMahon, A.P. (1993). Sonic hedgehog, a member of a family of putative signaling molecules, is implicated in the regulation of CNS polarity. *Cell* *75*, 1417–1430.
- Epps, D.E., Wolfe, M.L., and Groppi, V. (1994). Characterization of the steady-state and dynamic fluorescence properties of the potential-sensitive dye bis-(1,3-dibutylbarbituric acid)trimethine oxonol (DiBAC4(3)) in model systems and cells. *Chem. Phys. Lipids* *69*, 137–150.
- Farin, H.F., Jordens, I., Mosa, M.H., Basak, O., Korving, J., Tauriello, D.V., de Punder, K., Angers, S., Peters, P.J., Maurice, M.M., et al. (2016). Visualization of a short-range Wnt gradient in the intestinal stem-cell niche. *Nature* *530*, 340–343.
- Gong, X., Qian, H., Cao, P., Zhao, X., Zhou, Q., Lei, J., and Yan, N. (2018). Structural basis for the recognition of Sonic Hedgehog by human Patched1. *Science* *361*.
- Goodrich, L.V., Milenković, L., Higgins, K.M., and Scott, M.P. (1997). Altered neural cell fates and medulloblastoma in mouse patched mutants. *Science* *277*, 1109–1113.
- Hall, M.P., Unch, J., Binkowski, B.F., Valley, M.P., Butler, B.L., Wood, M.G., Otto, P., Zimmerman, K., Vidugiris, G., Machleidt, T., et al. (2012). Engineered luciferase reporter from a deep sea shrimp utilizing a novel imidazopyrazinone substrate. *ACS Chem. Biol.* *7*, 1848–1857.
- Hollway, G.E., Maule, J., Gautier, P., Evans, T.M., Keenan, D.G., Lohs, C., Fischer, D., Wicking, C., and Currie, P.D. (2006). Scube2 mediates Hedgehog signalling in the zebrafish embryo. *Dev. Biol.* *294*, 104–118.
- Huang, P., Nedelcu, D., Watanabe, M., Jao, C., Kim, Y., Liu, J., and Salic, A. (2016). Cellular cholesterol directly activates smoothed in hedgehog signaling. *Cell* *166*, 1176–1187.e14.
- Humke, E.W., Dorn, K.V., Milenkovic, L., Scott, M.P., and Rohatgi, R. (2010). The output of Hedgehog signaling is controlled by the dynamic association between Suppressor of Fused and the Gli proteins. *Genes Dev.* *24*, 670–682.
- Infante, R.E., Wang, M.L., Radhakrishnan, A., Kwon, H.J., Brown, M.S., and Goldstein, J.L. (2008). NPC2 facilitates bidirectional transfer of cholesterol between NPC1 and lipid bilayers, a step in cholesterol egress from lysosomes. *Proc. Natl. Acad. Sci. USA* *105*, 15287–15292.
- Ingham, P.W., and McMahon, A.P. (2001). Hedgehog signaling in animal development: paradigms and principles. *Genes Dev.* *15*, 3059–3087.
- Ingham, P.W., Nystedt, S., Nakano, Y., Brown, W., Stark, D., van den Heuvel, M., and Taylor, A.M. (2000). Patched represses the Hedgehog signalling pathway by promoting modification of the smoothed protein. *Curr. Biol.* *10*, 1315–1318.
- Iwamoto, H., Blakely, R.D., and De Felice, L.J. (2006). Na⁺, Cl⁻, and pH dependence of the human choline transporter (hCHT) in *Xenopus* oocytes:

- the proton inactivation hypothesis of hCHT in synaptic vesicles. *J. Neurosci.* **26**, 9851–9859.
- Kawakami, A., Nojima, Y., Toyoda, A., Takahoko, M., Satoh, M., Tanaka, H., Wada, H., Masai, I., Terasaki, H., Sakaki, Y., et al. (2005). The zebrafish-secreted matrix protein you/scube2 is implicated in long-range regulation of hedgehog signaling. *Curr. Biol.* **15**, 480–488.
- Kawakami, T., Kawcak, T., Li, Y.J., Zhang, W., Hu, Y., and Chuang, P.T. (2002). Mouse dispatched mutants fail to distribute hedgehog proteins and are defective in hedgehog signaling. *Development* **129**, 5753–5765.
- Kilambi, K.P., and Gray, J.J. (2012). Rapid calculation of protein pKa values using Rosetta. *Biophys. J.* **103**, 587–595.
- Krauss, S., Concorde, J.P., and Ingham, P.W. (1993). A functionally conserved homolog of the *Drosophila* segment polarity gene *hh* is expressed in tissues with polarizing activity in zebrafish embryos. *Cell* **75**, 1431–1444.
- Lee, H.C. (1984a). A membrane potential-sensitive Na⁺-H⁺ exchange system in flagella isolated from sea urchin spermatozoa. *J. Biol. Chem.* **259**, 15315–15319.
- Lee, H.C. (1984b). Sodium and proton transport in flagella isolated from sea urchin spermatozoa. *J. Biol. Chem.* **259**, 4957–4963.
- Luchetti, G., Sircar, R., Kong, J.H., Nachtergaele, S., Sagner, A., Byrne, E.F., Covey, D.F., Siebold, C., and Rohatgi, R. (2016). Cholesterol activates the G-protein coupled receptor smoothed to promote Hedgehog signaling. *eLife* **5**.
- Lum, L., and Beachy, P.A. (2004). The Hedgehog response network: sensors, switches, and routers. *Science* **304**, 1755–1759.
- Ma, Y., Erkner, A., Gong, R., Yao, S., Taipale, J., Basler, K., and Beachy, P.A. (2002). Hedgehog-mediated patterning of the mammalian embryo requires transporter-like function of dispatched. *Cell* **111**, 63–75.
- Murakami, S., Nakashima, R., Yamashita, E., Matsumoto, T., and Yamaguchi, A. (2006). Crystal structures of a multidrug transporter reveal a functionally rotating mechanism. *Nature* **443**, 173–179.
- Myers, B.R., Neahring, L., Zhang, Y., Roberts, K.J., and Beachy, P.A. (2017). Rapid, direct activity assays for smoothed reveal Hedgehog pathway regulation by membrane cholesterol and extracellular sodium. *Proc. Natl. Acad. Sci. USA* **114**, E11141–E11150.
- Myers, B.R., Sever, N., Chong, Y.C., Kim, J., Belani, J.D., Rychnovsky, S., Bazan, J.F., and Beachy, P.A. (2013). Hedgehog pathway modulation by multiple lipid binding sites on the smoothed effector of signal response. *Dev. Cell* **26**, 346–357.
- Nachtergaele, S., Whalen, D.M., Mydock, L.K., Zhao, Z., Malinauskas, T., Krishnan, K., Ingham, P.W., Covey, D.F., Siebold, C., and Rohatgi, R. (2013). Structure and function of the smoothed extracellular domain in vertebrate Hedgehog signaling. *eLife* **2**, e01340.
- Nakano, Y., Guerrero, I., Hidalgo, A., Taylor, A., Whittle, J.R., and Ingham, P.W. (1989). A protein with several possible membrane-spanning domains encoded by the *Drosophila* segment polarity gene *patched*. *Nature* **341**, 508–513.
- Nakano, Y., Kim, H.R., Kawakami, A., Roy, S., Schier, A.F., and Ingham, P.W. (2004). Inactivation of dispatched 1 by the chameleon mutation disrupts Hedgehog signalling in the zebrafish embryo. *Dev. Biol.* **269**, 381–392.
- Nedelcu, D., Liu, J., Xu, Y., Jao, C., and Salic, A. (2013). Oxysterol binding to the extracellular domain of smoothed in Hedgehog signaling. *Nat. Chem. Biol.* **9**, 557–564.
- Nikaido, H. (2018). RND transporters in the living world. *Res. Microbiol.* **169**, 363–371.
- Ohana, R.F., Encell, L.P., Zhao, K., Simpson, D., Slater, M.R., Urh, M., and Wood, K.V. (2009). HaloTag7: a genetically engineered tag that enhances bacterial expression of soluble proteins and improves protein purification. *Protein Expr. Purif.* **68**, 110–120.
- Pauly, D., Chacana, P.A., Calzado, E.G., Brembs, B., and Schade, R. (2011). IgY technology: extraction of chicken antibodies from egg yolk by polyethylene glycol (PEG) precipitation. *J. Vis. Exp.* **51**.
- Pepinsky, R.B., Zeng, C., Wen, D., Rayhorn, P., Baker, D.P., Williams, K.P., Bixler, S.A., Ambrose, C.M., Garber, E.A., Miatkowski, K., et al. (1998). Identification of a palmitic acid-modified form of human Sonic hedgehog. *J. Biol. Chem.* **273**, 14037–14045.
- Porter, J.A., Young, K.E., and Beachy, P.A. (1996). Cholesterol modification of hedgehog signaling proteins in animal development. *Science* **274**, 255–259.
- Pos, K. (2009). Drug transport mechanism of the AcrB efflux pump. *Biochim Biophys Acta* **1794**, 782–793.
- Qi, X., Schmiede, P., Coutavas, E., and Li, X. (2018a). Two Patched molecules engage distinct sites on Hedgehog yielding a signaling-competent complex. *Science* **362**.
- Qi, X., Schmiede, P., Coutavas, E., Wang, J., and Li, X. (2018b). Structures of human Patched and its complex with native palmitoylated sonic hedgehog. *Nature* **560**, 128–132.
- Qian, H., Cao, P., Hu, M., Gao, S., Yan, N., and Gong, X. (2019). Inhibition of tetrameric Patched1 by Sonic Hedgehog through an asymmetric paradigm. *Nat. Commun.* **10**, 2320.
- Reeves, P.J., Callewaert, N., Contreras, R., and Khorana, H.G. (2002). Structure and function in rhodopsin: high-level expression of rhodopsin with restricted and homogeneous N-glycosylation by a tetracycline-inducible N-acetylglucosaminyltransferase I-negative HEK293S stable mammalian cell line. *Proc. Natl. Acad. Sci. USA* **99**, 13419–13424.
- Riddle, R.D., Johnson, R.L., Laufer, E., and Tabin, C. (1993). Sonic hedgehog mediates the polarizing activity of the ZPA. *Cell* **75**, 1401–1416.
- Rohatgi, R., Milenkovic, L., and Scott, M.P. (2007). Patched1 regulates hedgehog signaling at the primary cilium. *Science* **317**, 372–376.
- Rubin, L.L., and de Sauvage, F.J. (2006). Targeting the Hedgehog pathway in cancer. *Nat. Rev. Drug Discov.* **5**, 1026–1033.
- Seeger, M.A., Schiefner, A., Eicher, T., Verrey, F., Diederichs, K., and Pos, K.M. (2006). Structural asymmetry of AcrB trimer suggests a peristaltic pump mechanism. *Science* **313**, 1295–1298.
- Su, C.C., Li, M., Gu, R., Takatsuka, Y., McDermott, G., Nikaido, H., and Yu, E.W. (2006). Conformation of the AcrB multidrug efflux pump in mutants of the putative proton relay pathway. *J. Bacteriol.* **188**, 7290–7296.
- Taipale, J., Cooper, M.K., Maiti, T., and Beachy, P.A. (2002). Patched acts catalytically to suppress the activity of smoothed. *Nature* **418**, 892–897.
- Takatsuka, Y., and Nikaido, H. (2006). Threonine-978 in the transmembrane segment of the multidrug efflux pump AcrB of *Escherichia coli* is crucial for drug transport as a probable component of the proton relay network. *J. Bacteriol.* **188**, 7284–7289.
- Tukachinsky, H., Kuzmickas, R.P., Jao, C.Y., Liu, J., and Salic, A. (2012). Dispatched and scube mediate the efficient secretion of the cholesterol-modified hedgehog ligand. *Cell Rep.* **2**, 308–320.
- Tukachinsky, H., Lopez, L.V., and Salic, A. (2010). A mechanism for vertebrate Hedgehog signaling: recruitment to cilia and dissociation of SuFu-Gli protein complexes. *J. Cell Biol.* **191**, 415–428.
- Tukachinsky, H., Petrov, K., Watanabe, M., and Salic, A. (2016). Mechanism of inhibition of the tumor suppressor Patched by Sonic Hedgehog. *Proc. Natl. Acad. Sci. USA* **113**, E5866–E5875.
- van den Heuvel, M., and Ingham, P.W. (1996). smoothed encodes a receptor-like serpentine protein required for hedgehog signalling. *Nature* **382**, 547–551.
- Wang, X., Moon, J., Dodge, M.E., Pan, X., Zhang, L., Hanson, J.M., Tuladhar, R., Ma, Z., Shi, H., Williams, N.S., et al. (2013). The development of highly potent inhibitors for porcupine. *J. Med. Chem.* **56**, 2700–2704.
- Waterhouse, A.M., Procter, J.B., Martin, D.M., Clamp, M., and Barton, G.J. (2009). Jalview Version 2—a multiple sequence alignment editor and analysis workbench. *Bioinformatics* **25**, 1189–1191, version 2.
- Woods, I.G., and Talbot, W.S. (2005). The you gene encodes an EGF-CUB protein essential for Hedgehog signaling in zebrafish. *PLoS Biol.* **3**, e66.
- Zhang, Y., Bulkley, D.P., Xin, Y., Roberts, K.J., Asarnow, D.E., Sharma, A., Myers, B.R., Cho, W., Cheng, Y., and Beachy, P.A. (2018). Structural basis for cholesterol transport-like activity of the hedgehog receptor patched. *Cell* **175**, 1352–1364.e14.

STAR★METHODS

KEY RESOURCES TABLE

REAGENT or RESOURCE	SOURCE	IDENTIFIER
Antibodies		
rabbit monoclonal anti-SHH (clone C9C5)	Cell Signaling Technology	Cat# 2207S; RRID: AB_2188191
rabbit monoclonal anti-WNT3A (clone C64F2)	Cell Signaling Technology	Cat# 2721; RRID: AB_2215411
rabbit polyclonal anti-GFP	Rockland	Cat# 600-401-215; RRID: AB_828167
mouse monoclonal anti-tubulin (clone DM1A)	Sigma; Blose et al., 1984	Cat# T6199; RRID: AB_477583
mouse monoclonal anti-acetylated tubulin (clone 6-11B-1)	Sigma	Cat# T7451; RRID: AB_609894
goat polyclonal anti-mSMO	Nedelcu et al., 2013	N/A
rabbit polyclonal anti-mCherry	Nedelcu et al., 2013	N/A
chicken polyclonal anti-mARL13B	This study	N/A
rat anti-HA (clone 3F10)-HRP conjugate	Roche	Cat# 12013819001; RRID: AB_390917
sheep anti-mouse IgG-HRP conjugate	Jackson ImmunoResearch	Cat# 515-005-003; RRID: AB_2340287
donkey anti-rabbit IgG-HRP conjugate	GE Healthcare	Cat# NA934; RRID: AB_772206
donkey anti-goat IgG-Alexa Fluor 488 conjugate	Thermo	Cat# A-11055; RRID: AB_2534102
donkey anti-rabbit IgG-Alexa Fluor 555 conjugate	Thermo	Cat# A-31572; RRID: AB_162543
donkey anti-chicken IgY-Alexa Fluor 647 conjugate	Jackson ImmunoResearch	Cat# 703-605-155; RRID: AB_2340379
Bacterial and Virus Strains		
<i>E. coli</i> BL21 (DE3) pLysS	Sigma	Cat# 69451
Chemicals, Peptides, and Recombinant Proteins		
polyethylenimine (PEI), linear, MW 25000	Polysciences	Cat# 23966
TransIT-293 Transfection Reagent	Mirus	Cat# MIR2700
cycloheximide (≥ 94%)	Sigma	Cat# C7698
methyl-β-cyclodextrin (MβCD)	Sigma	Cat# 332615
IWP-2 (PORCN inhibitor) (≥ 98%)	Sigma; Wang et al., 2013	Cat# I0536
SAG (SMO agonist) (≥ 98%)	Axxora; Chen et al., 2002	Cat# BV-1939
SANT-1 (SMO antagonist) (≥ 95%)	Calbiochem; Chen et al., 2002	Cat# 559303
gramicidin A	Sigma	Cat# 50845
veratridine (≥ 98%)	Tocris Bioscience	Cat# 2918
bis-(1,3-dibutylbarbituric acid) trimethine oxonol (DIBAC ₄ (3)) (≥ 95%)	Sigma	Cat# D8189
carbonyl cyanide 3-chlorophenylhydrazone (CCCP) (≥ 97%)	Sigma	Cat# C2759
staurosporine (>99%)	LC Laboratories	Cat# S-9300
oligomycin A (≥ 99%)	Sigma	Cat# 75351
See Table S1 for composition of modified Tyrode's media utilized in this study	This study	N/A
FLAG peptide: NH ₂ -DYKDDDDK-OH	Genscript	N/A
6xHis-mARL13B (antigen for immunization)	This study	N/A
MBP-mARL13B (for antibody affinity purification)	This study	N/A
FLAG-HT7-mSCUBE2-ΔFurin	This study	N/A

(Continued on next page)

Continued

REAGENT or RESOURCE	SOURCE	IDENTIFIER
Critical Commercial Assays		
MiSeq Reagent Kit v2	Illumina	Cat# MS-102-2001
Affi-Gel 10 Gel	Bio-Rad	Cat# 1536099
anti-FLAG M1 resin	Millipore	Cat# A4596
Amicon Ultra-4 Centrifugal Filter Unit – 10kDa cutoff	Millipore	Cat# UFC8010
Superdex 200, 10/300 GL	GE Healthcare	Cat# 17517501
Nano-Glo Luciferase Assay	Promega	Cat# N1120
BCA Assay	G Biosciences	Cat# 786-570
TRIzol Reagent	Thermo	Cat# 15596018
RQ1 RNase-Free DNase	Promega	Cat# M6101
LunaScript RT SuperMix Kit	NEB	Cat# E3010L
PowerUp SYBR Green Master Mix	Thermo	Cat# A25742
CellTiter-Glo Luminescent Cell Viability Assay	Promega	Cat# G7572
MTT Cell Proliferation Assay Kit	Cayman Chemical	Cat# 10009365
Experimental Models: Cell Lines		
Human: HEK293T	ATCC	Cat# CRL-3216; RRID: CVCL_0063
Human: HEK293S GnTI ⁻	A.C. Kruse; ATCC; Reeves et al., 2002	Cat# CRL-3022; RRID: CVCL_A785
Mouse: L cell	ATCC	Cat# CRL-2648; RRID: CVCL_4536
Mouse: L Wnt-3A	ATCC	Cat# CRL-2647; RRID: CVCL_0635
Mouse: NIH-3T3	ATCC	Cat# CRL-1658; RRID: CVCL_0594
Mouse: <i>Ptch1</i> ^{-/-} MEF	Goodrich et al., 1997	N/A
Human: <i>DISP1</i> ^{KO} HEK293T	This study	N/A
Oligonucleotides		
<i>mRpl27</i> qRT-PCR forward primer: 5'-GTCGAGATGGGCAAGTTCAT-3'	Nedelcu et al., 2013	N/A
<i>mRpl27</i> qRT-PCR reverse primer: 5'-GCTTGGCGATCTTCTTCTTG-3'	Nedelcu et al., 2013	N/A
<i>mGli1</i> qRT-PCR forward primer: 5'-GGCCAATCACAAGTCAAGGT-3'	Nedelcu et al., 2013	N/A
<i>mGli1</i> qRT-PCR reverse primer: 5'-TTCAGGAGGAGGGTACAACG-3'	Nedelcu et al., 2013	N/A
See Table S2 for a list of CRISPR gRNA oligonucleotides and sequencing primers utilized in this study	This study	N/A
Recombinant DNA		
See Table S3 for a list of all plasmids utilized in this study	This study	N/A
Software and Algorithms		
MetaMorph Microscopy Automation and Image Analysis Software	Molecular Devices	http://www.moleculardevices.com/Products/Software/Meta-Imaging-Series/MetaMorph.html ; RRID: SCR_002368
MATLAB	MathWorks	http://www.mathworks.com/products/matlab/ ; RRID: SCR_001622
FIJI	National Institutes of Health	http://fiji.sc/ ; RRID: SCR_002285

(Continued on next page)

Continued

REAGENT or RESOURCE	SOURCE	IDENTIFIER
JalView	Waterhouse et al., 2009	http://www.jalview.org/ ; RRID: SCR_006459
PyMOL	Schrodinger	http://www.pymol.org/ ; RRID:SCR_000305
Prism 8	GraphPad	http://www.graphpad.com/ ; RRID: SCR_002798
Photoshop CS5	Adobe	https://www.adobe.com/products/photoshop.html ; RRID: SCR_014199
Inkscape	Inkscape	https://inkscape.org/en/ ; RRID: SCR_014479

RESOURCE AVAILABILITY

Lead Contact

Further information and requests for reagents should be directed to, and will be fulfilled by, the Lead Contact, Adrian Salic (asalic@hms.harvard.edu).

Materials Availability

All newly generated plasmids and cell lines are available from the Lead Contact upon request.

Data and Code Availability

This study did not generate datasets. Custom MATLAB scripts utilized for image analysis are available from the Lead Contact upon request.

EXPERIMENTAL MODEL AND SUBJECT DETAILS

Cell Culture

HEK293T, HEK293S GnTI⁻, NIH-3T3, and L cells were purchased from ATCC. L cells, HEK293T and HEK293S GnTI⁻ cells, and Ptch1^{-/-} MEFs (Goodrich et al., 1997) were grown in Dulbecco's Modified Eagle's Medium (DMEM) with 10% fetal bovine serum (FBS), penicillin, and streptomycin. NIH-3T3 cells were grown in DMEM with 10% bovine calf serum (BCS), penicillin, and streptomycin. HEK293T and HEK293S GnTI⁻ cells are female. NIH-3T3 and L cells are male. The sex of Ptch1^{-/-} MEFs has not been determined. Stable lines were generated by lentiviral transduction, followed by blasticidin selection (50 μg/mL), as described (Tukachinsky et al., 2012). Briefly, HEK293T cells were transiently transfected (*TransIT*-293, Mirus) with lentiviral constructs bearing transgenes of interest; lentivirus-conditioned medium was harvested after 48 h and used to infect cells of interest. For transient expression experiments, cells were transfected using polyethylenimine (PEI, Polysciences). For SHH-NL5 titration experiments, the amount of transfected DNA was equalized by mixing the SHH-NL5 expression construct with carrier plasmid DNA (pBluescript).

Generation of *DISP1* Knockout (*DISP1*^{KO}) HEK293T Cells by CRISPR/Cas9

Two gRNA sequences were chosen, in exons 2 and 4 (the first and third exons with coding sequence) of human *DISP1* (crispr.mit.edu). Targeting constructs were generated in a derivative of pX330 (Cong et al., 2013) expressing EGFP-tagged Cas9. HEK293T cells were co-transfected with the two targeting plasmids, and EGFP-positive cells, isolated by fluorescence-activated sorting, were plated clonally. Genomic DNA was extracted from single clones and was initially screened by PCR, to identify cells with large deletions spanning the two gRNA-targeted loci. A clonal line harboring a 47.7-kbp deletion allele was identified. Both gRNA loci were then PCR amplified and Sanger sequenced to define all lesions present. Lesions were further confirmed by sequencing target locus amplicons on a MiSeq instrument (Illumina). The *DISP1*^{KO} line used in this study harbors a deletion allele, as well as alleles with frameshifts at both targeted loci. Two indels causing frameshifts were identified at the exon 2 locus, and one indel causing frameshift at the exon 4 locus. No wild-type sequences were observed by MiSeq at either locus. That two frameshifts were identified for exon 2 perhaps reflects the presence of 3 copies of the *DISP1* locus in HEK293T cells.

METHOD DETAILS

Antibodies

The following antibodies were purchased: rabbit anti-SHH monoclonal antibody (Cell Signaling Technology), rabbit anti-WNT3A monoclonal antibody (Cell Signaling Technology), rabbit anti-GFP polyclonal antibody (Rockland), mouse monoclonal anti-tubulin (Sigma), mouse anti-acetylated tubulin monoclonal antibody (Sigma), rat anti-HA-HRP conjugate (Roche), sheep anti-mouse

IgG–HRP conjugate (Jackson ImmunoResearch), donkey anti-rabbit IgG–HRP conjugate (GE Healthcare), donkey anti-goat IgG–Alexa Fluor 488 conjugate (Thermo), donkey anti-rabbit IgG–Alexa Fluor 555 conjugate (Thermo), and donkey anti-chicken IgY–Alexa Fluor 647 conjugate (Jackson ImmunoResearch). Antibodies against mCherry (Nedelcu et al., 2013) and against mouse SMO (Tukachinsky et al., 2010) were described previously. Polyclonal antibodies against mouse ARL13B (mARL13B), a marker of cilia, were raised in chickens. Briefly, 6xHis-tagged mARL13B was expressed in *E. coli* (BL21 DE3 pLysS, Novagen), was purified as a soluble protein, and was used to immunize hens (Abcore). Whole IgY was isolated from eggs laid by the immunized hens, as described (Pauly et al., 2011). Anti-mARL13B antibodies were isolated from whole IgY, by affinity purification against recombinant MBP-tagged mARL13B immobilized on Affi-Gel 10 beads (Bio-Rad).

DNA Constructs

All constructs were subcloned into a lentiviral CMV promoter-driven expression vector. Overlapping PCR was used to introduce mutations and to assemble fusions, and the resulting constructs were confirmed by sequencing. Mouse DISP1 and PTCH1 were tagged with mCherry fluorescent protein at their C-termini. SHH-NL fusions were generated by inserting the coding sequence for NanoLuc (NL, Promega), flanked by two glycine residues on either end, between the following residues of the N-terminal signaling domain of human SHH: K32 and R33; N69 and S70; S70 and E71; P82 and D83; N91 and T92; P118 and G119; E130 and D131; R153 and D154; K194 and S195. WNT3A-NL consists of the influenza hemagglutinin signal sequence, one copy of the FLAG epitope, the NL sequence, followed by the sequence of mouse WNT3A without signal sequence; this is the same tagging location as used to generate epitope-tagged functional WNT3A (Farin et al., 2016). The expression construct for producing mouse SCUBE2 contained, from the N terminus: the influenza hemagglutinin signal sequence, one copy of the FLAG epitope, the mutant bacterial dehalogenase HaloTag7 (Ohana et al., 2009), a PreScission protease cleavage site, and the sequence of SCUBE2 without the signal sequence. To increase the yield of full-length SCUBE2, the putative furin cleavage site was mutated (R274A, R276A, R277A).

Custom Media Formulations

Cell culture media of defined ionic composition were based on Tyrode's solution, and are described in Table S1.

Fluorescence-Activated Cell Sorting

A single-cell suspension at 10×10^6 cells per mL in phenol red-free DMEM, supplemented with 0.5% FBS was made by trypsinizing, pelleting, and resuspending cells. The suspension was passed through a $35 \mu\text{m}$ nylon strainer and cells were sorted on a FACSAria III (BD Biosciences) cell sorter equipped with a 561nm yellow laser and multi-sort option. The population fluorescence distribution was measured for each population after the sort.

Protein Expression and Purification

SCUBE2 was affinity purified on anti-FLAG-M1 resin (Millipore), from media conditioned by HEK293S GnT1⁻ cells stably transduced with the SCUBE2-expressing lentivirus. Briefly, conditioned media was clarified by centrifugation and filtration, and was then adjusted to 300 mM NaCl, 2 mM CaCl₂, and 0.1% Triton X-100. The media was applied twice to a column packed with anti-FLAG-M1 resin, at 4°C. The column was washed with >10 column volumes of wash buffer with detergent (10 mM Tris pH 8, 150 mM NaCl, 2mM CaCl₂, 0.1% Triton X-100), followed by >20 column volumes of wash buffer without detergent (10 mM Tris pH 8, 150 mM NaCl, 2mM CaCl₂). The protein was eluted at room temperature, with 100 $\mu\text{g}/\text{mL}$ FLAG peptide (Genscript) in Tris-buffered saline (TBS, 10 mM Tris pH 8, 150 mM NaCl). Fractions containing the protein were pooled and concentrated using centrifugal concentrators (Millipore), according to the manufacturer's instructions. SCUBE2 was further purified by gel filtration on a Superdex 200 column (GE Healthcare).

Luciferase-based SHH Release Assays

HEK293T cells stably expressing SHH-NL5 were plated on poly-D-lysine, in complete media. The next day, the cells were exchanged into DMEM, and were cultured overnight. The cells were washed three times with DMEM, to remove all serum, and were preincubated with cycloheximide (100 $\mu\text{g}/\text{mL}$, Sigma) for 30 min. The release reaction was started by switching the cells into media supplemented with purified SCUBE2, BSA (negative control), or methyl- β -cyclodextrin (M β CD, Sigma), in the continued presence of cycloheximide. The cells were incubated at 37°C in a cell culture incubator, and aliquots of the supernatant were withdrawn at specified time points. Between time points, the plates were gently shaken to ensure even mixing of media. Collected supernatants were centrifuged, to remove possible cellular debris, and NanoLuc activity was measured on a Wallac Victor3 Microplate Reader (Perkin-Elmer), using Nano-Glo Luciferase Assay Substrate (Promega), according to the manufacturer's instructions. Luminescence measurements were corrected for the decreasing supernatant volume during the assay. Only linear portions of release curves were used to calculate initial release rates. In experiments comparing SHH-NL5 release between different cell lines, the cells were also harvested at the end of the experiment (30 min), were lysed in TBS with 0.2% Triton X-100, and NanoLuc activity was measured, to determine SHH-NL5 expression levels. Only a small fraction (<5%) of total SHH-NL5 was released from cells during the 30-minute duration of the release assay. Specific modifications of this protocol used during initial assay development are noted in the associated figure legends. Luminescence dynamic range and standard curves were determined using recombinant NanoLuc, expressed and purified from bacteria.

WNT3A Release Assays

L cells stably expressing WNT3A or WNT3A-NL were grown overnight in complete media, and were washed thrice with DMEM. The cells were then incubated overnight in DMEM without serum or with 10% FBS, in the absence or presence of the Porcupine (PORCN) inhibitor, IWP-2 (2 μ M, Sigma). Media was harvested, was centrifuged to remove cellular debris, and released WNT3A was detected by SDS-PAGE and immunoblotting, while released WNT3A-NL was measured by luminescence, as for SHH-NL5. Total WNT3A-NL was measured in cell lysates, as for SHH-NL5. For measuring the effect of the Na⁺ gradient on WNT3A-NL release rates, after washing with DMEM, the cells were preincubated in DMEM with cycloheximide (100 μ g/mL) for 30 min, after which WNT3A-NL release was initiated by switching cells into the indicated Tyrode's media, supplemented with cycloheximide and 2% FBS. Aliquots of the supernatant were withdrawn at specified time points, and released WNT3A-NL was measured as above. Remaining WNT3A-NL was measured in cell lysates.

Total Protein Measurements

Total protein was measured using a BCA assay (G Biosciences), according to manufacturer's recommendations, using cell lysates harvested at the end of each experiment (see above). Briefly, 5–10 μ L of cell lysate was combined with 1 mL BCA reagent and incubated at 37°C for 60 min. Absorbance was read at 562 nm using a Cary 300 UV-Vis spectrophotometer (Agilent). Protein concentration was determined according to a BSA standard curve.

Immunoblot-based SHH Release

On day 1, wild-type or *DISP1*^{KO} HEK293T cells were plated in 6-well format, such that they would reach 50% confluence the next day. On day 2, cells were transiently transfected with SHH and the indicated SCUBE2 and DISP1 constructs. On day 3, the cells were washed three times with DMEM at 2-hour intervals to remove serum and then into DMEM for overnight collection. Conditioned media was harvested, centrifuged to remove debris, and then subjected to trichloroacetic acid (TCA) precipitation. Precipitated proteins were separated by SDS-PAGE, and released SHH was detected by immunoblotting (Tukachinsky et al., 2012).

Microscopy and Immunofluorescence

On day 1, cells were plated on gelatin-coated glass coverslips, such that they would reach confluence the next day. On day 2, the cells were serum-starved, by overnight incubation in DMEM. On day 3, the cells were incubated under the indicated conditions, after which they were fixed with 3.7% formaldehyde in phosphate-buffered saline (PBS, 10 mM Na₂HPO₄, 1.8 mM KH₂PO₄, 2.7 mM KCl, 137 mM NaCl) at room temperature, for 15 min. The cells were washed with TBS, were permeabilized with TBST (TBS with 0.2% Triton X-100), and were incubated in a blocking solution (25 mg/mL BSA in TBST). Immunofluorescence was performed as described (Tukachinsky et al., 2010). The primary antibodies were: chicken anti-ARL13B, rabbit anti-mCherry, goat anti-SMO, each at 2 μ g/mL final concentration. The secondary antibodies were: donkey anti-goat IgG–Alexa Fluor 488 conjugate, donkey anti-rabbit IgG–Alexa Fluor 555 conjugate, donkey anti-chicken IgY–Alexa Fluor 647, each at 1 μ g/mL final concentration. Images were acquired with a 40x Plan Apo 0.95 N.A. objective lens (Nikon), on a TE2000E microscope (Nikon) equipped with a motorized stage (Prior Scientific) and an OrcaER camera (Hamamatsu Photonics). Ciliary fluorescence intensity was quantified using custom-built scripts implemented in MATLAB, as described (Nedelcu et al., 2013). At least 100 cilia were analyzed per condition. Details of statistical testing are described in figure legends.

Quantitative RT-PCR

Measurements of *Gli1* expression, relative to the housekeeping gene *Rpl27*, were done by quantitative RT-PCR, as described (Tukachinsky et al., 2016). Briefly, cells were serum-starved overnight and treated as described in the figure legends. TRIzol (Thermo) was used to extract total RNA, which was treated with DNase I (Promega) and re-extracted with TRIzol prior to reverse transcription (LunaScript RT SuperMix, NEB). cDNA samples were quantified with PowerUp SYBR Green Master Mix (Thermo) and the indicated primers (Key Resources Table). Biological triplicates were performed for all assays.

E_m Measurements

DiBAC₄(3) (Sigma), a dye with E_m-sensitive uptake (Epps et al., 1994), was used to measure E_m for cells incubated in various media. Confluent NIH-3T3 cells were serum-starved in DMEM for 4–6 h, after which the cells were detached by trypsinization, were washed, and the cell suspension was incubated with DiBAC₄(3) (400 nM), for 30 min at 37°C. The cells were then analyzed on a FACSCalibur flow cytometer (BD Biosciences), using 488 nm laser excitation and a 530/30 emission filter. Media with various K⁺ concentrations were used as positive controls for membrane depolarization. A standard curve for DiBAC₄(3) fluorescence was determined by permeabilizing cells with 2 μ g/mL gramicidin A (Sigma), incubating them with DiBAC₄(3) (0, 25, 50, 100, 200, 400 nM), followed by fluorescence measurement by flow cytometry.

Cellular ATP Measurements

NIH-3T3 cells were plated in 96-well plates, at a density of 40,000 cells per well. The next day, the complete media was replaced with DMEM, followed by overnight incubation. The cells were washed again with DMEM and were then incubated in media of defined ionic composition, for 3 or 6 h. After the incubation period, cellular ATP was measured using the CellTiter-Glo reagent (Promega), according to manufacturer's instructions, using a Wallac Victor3 Microplate Reader. As a control, cellular ATP was depleted by incubation in

PBS supplemented with CCCP (1 μ M or 5 μ M, as indicated; Sigma), staurosporine (2 μ M, LC Laboratories), or oligomycin A (100nM, Sigma). Standard curves were determined using pure ATP solutions. All ATP measurements were performed at least three times.

Cellular NAD(P)H Measurements

NAPD(P)H was assayed using an MTT viability assay (Cayman Chemical). HEK293T cells were plated on poly-D-lysine coated 96-well plates, at a density of 50,000 cells per well. The next day, cells were gently washed with DMEM (0.1 mL/well) and were incubated in test media for 3 h. The media was then removed and PBS (0.1 mL/well) and MTT reagent (5 μ L/well) were added, followed by incubation at 37°C for 3 h. The dissolution solution (0.1 mL/well) was then added, followed by incubation at room temperature overnight. The next day, absorbance at 570nm was read using a microplate reader.

Kinetic Model for DISP1-catalyzed SHH Release

We hypothesized that DISP1 acts as an enzyme in SHH release. This scenario is described by the following scheme:



SHH and SCUBE2 (added purified protein) are substrates for DISP1, while SCUBE2:SHH (i.e., released SHH) is the reaction product. We apply an equilibrium assumption, that binding is faster than enzyme kinetics, which means that we can describe the concentrations of intermediate species according to their binding equilibria:

$$[\text{SHH} : \text{DISP1}] = \frac{[\text{SHH}][\text{DISP1}]}{K_{d1}}$$

$$[\text{SCUBE2} : \text{DISP1}] = \frac{[\text{SCUBE2}][\text{DISP1}]}{K_{d2}}$$

The ternary complex SHH:SCUBE2:DISP1 can form either by SCUBE2 joining SHH:DISP1, or by SHH joining SCUBE2:DISP1, hence two Michaelis–Menten constants, K_{M1} and K_{M2} , respectively. Importantly, the rate of SHH release (v_{release}) does not depend on the order of the substrate association with DISP1. Putting everything together, we obtain:

$$v_{\text{release}} = \frac{V_{\text{max}}}{1 + \frac{K_{M1}}{[\text{SCUBE2}]} + \frac{K_{M2}}{[\text{SHH}]} + \frac{K_{d1}K_{M2}}{[\text{SCUBE2}][\text{SHH}]}} \quad (\text{Equation 1})$$

where $V_{\text{max}} = [\text{DISP1}] * k_{\text{cat}}$.

Rearranging Equation 1 to show the release rate dependence on [SCUBE2], we have:

$$v_{\text{release}} = \frac{V_{\text{max}}[\text{SCUBE2}]}{K_M + [\text{SCUBE2}] \left(1 + \frac{K_{M2}}{[\text{SHH}]} \right)} \quad (\text{Equation 2})$$

where $K_M = K_{M1} + \frac{K_{d1}K_{M2}}{[\text{SHH}]}$.

In most of our experiments, SHH is saturating, i.e., $[\text{SHH}] \gg K_{M2}$. This yields Equation 3:

$$v_{\text{release}} = \frac{V_{\text{max}}[\text{SCUBE2}]}{K_{M1} + [\text{SCUBE2}]} \quad (\text{Equation 3})$$

Equation 3 predicts that the release rate will saturate as a function of [SCUBE2], which is what is observed (Figure 2E). This shows that SHH release by SCUBE2 is a catalyzed process, as opposed to a simple binding equilibrium.

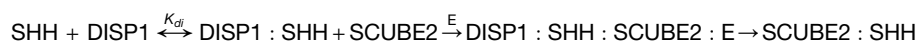
According to Equation 3, if DISP1 were the enzyme catalyzing SHH release, then V_{max} , but not K_M , would be a function of [DISP1], since:

$$V_{\text{max}} = [\text{DISP1}] * k_{\text{cat}}$$

We test this prediction by varying [DISP1] (Figures 2F–2K, and S2H–S2J), and we find that DISP1 levels indeed affect V_{max} , but not K_M , which remains constant at 2–3 μ M across multiple independent experiments. These results strongly suggest that DISP1 is the rate-limiting enzyme that catalyzes SHH release.

Kinetic Model for DISP1 Playing an Accessory Role in SHH Release

As an alternative hypothesis, we considered a second scheme, wherein DISP1 functions as an adaptor between membrane-bound SHH and an unknown enzyme (E) catalyzing SCUBE2:SHH release. This scenario is described by the following scheme:



Applying an equilibrium assumption as above, we obtain the following:

$$[\text{SHH} : \text{DISP1}] = \frac{[\text{SHH}][\text{DISP1}]}{K_{d1}}$$

$$[\text{SHH} : \text{DISP1} : \text{E}] = \frac{[\text{SHH} : \text{DISP1}][\text{E}]}{K_{d1}} = \frac{[\text{SHH}][\text{DISP1}][\text{E}]}{K_{d1}K_{d1}}$$

$$\text{SCUBE2} : \text{E} = \frac{[\text{SCUBE2}][\text{E}]}{K_{d2}}$$

Michaelis–Menten constants are similar to those above, with K_{M1} describing SCUBE2 joining the enzyme:substrate complex and K_{M2} describing SHH:DISP1 joining the enzyme substrate complex; k_{cat} is the catalytic constant of the enzyme E. The resulting rate equation is:

$$v_{\text{release}} = \frac{V_{\text{max}}}{1 + \frac{K_{M1}}{[\text{SCUBE2}]} + \frac{K_{M2}K_{d1}}{[\text{SHH}][\text{DISP1}]} + \frac{K_{M1}K_{M2}K_{d1}}{[\text{SCUBE2}][\text{SHH}][\text{DISP1}]}} \quad (\text{Equation 4})$$

where $V_{\text{max}} = [\text{E}] \cdot k_{\text{cat}}$.

Rearranging [Equation 4](#) to show the release rate dependence on [SCUBE2], we have:

$$v_{\text{release}} = \frac{V_{\text{max}}[\text{SCUBE2}]}{K_M^* + [\text{SCUBE2}] \left(1 + \frac{K_{M2}K_{d1}}{[\text{SHH}][\text{DISP1}]} \right)} \quad (\text{Equation 5})$$

where $K_M^* = K_{M1} + \frac{K_{d1}K_{M2}K_{d1}}{[\text{SHH}][\text{DISP1}]}$.

This scenario also predicts release rate saturation as a function of SCUBE2; however, now the measured K_M (K_M^*), but not V_{max} , would be a function of [DISP1]. This is the opposite of what we observe experimentally, indicating that DISP1 itself, not another enzyme, catalyzes SHH release.

Calculations of the Electrochemical Driving Force (EDF)

The EDF for Na^+ and K^+ for the experiments in [Figures 3E](#) and [3F](#) was calculated using [Equation E1](#):

$$\text{EDF}_{\text{Na}^+} = E_m - \frac{RT}{F} \ln \left(\frac{[\text{Na}^+]_{\text{out}}}{[\text{Na}^+]_{\text{in}}} \right) \quad (\text{Equation E1})$$

where R is the universal gas constant, $T=300\text{K}$, F is the Faraday constant, and E_m is the resting membrane potential. E_m was estimated using the Goldman–Hodgkin–Katz equation, assuming a ratio of 10:1 in $\text{Na}^+:\text{K}^+$ permittivity, $[\text{Na}^+]_{\text{in}} = 15\text{mM}$, $[\text{K}^+]_{\text{in}}=125\text{mM}$, $[\text{Cl}^-]_{\text{in}}=15\text{mM}$.

Blot Image Processing

Blot images in which species of different molecular weights were probed simultaneously were cropped in Photoshop CS5. Where necessary, such blots were resized along the horizontal axis to present clear vertical alignment of lanes across multiple probed species. Original images are available upon request.

QUANTIFICATION AND STATISTICAL ANALYSIS

SHH release was measured as a single measurement over multiple time points unless indicated otherwise in the figure legends. The release rate was calculated as the slope of the linear regression line fit to the linear portion, typically 1–30min, of the SHH release data. Curve fitting was performed in Prism 8 (GraphPad Software), using least-squares linear or nonlinear regression, as indicated in the figure legends. Parameter estimates are reported with associated standard errors of the estimate. Statistical tests and associated significance threshold are reported in the figure legends.

Developmental Cell, Volume 55

Supplemental Information

Distinct Cation Gradients Power

Cholesterol Transport at Different Key Points

in the Hedgehog Signaling Pathway

Kostadin Petrov, Bradley M. Wierbowski, Jingjing Liu, and Adrian Salic

Figure S1

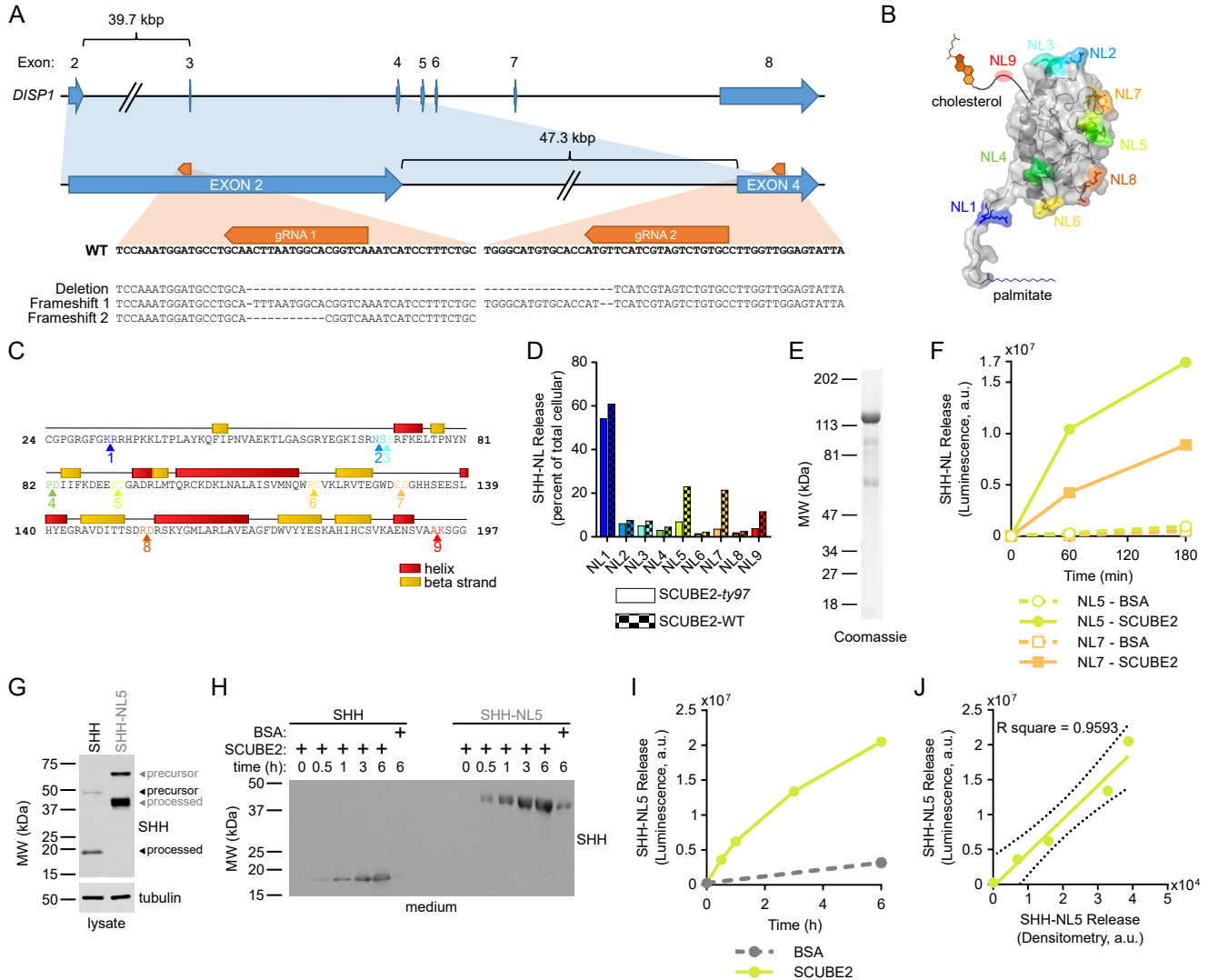


Figure S1. Generation of *DISP1*^{KO} cells and SHH-NanoLuc (SHH-NL) fusions, related to Figures 1 and 2

(A) Top: map of the human *DISP1* genomic locus, showing the two guide RNAs (gRNAs) used to generate *DISP1*^{KO} HEK293T cells. Bottom: sequence of the three *DISP1* alleles in the *DISP1*^{KO} clone used in this study.

(B) Schematic of the human SHH ligand (PDB: 6e1h.c), showing the 9 sites where NanoLuc luciferase (NL) was inserted.

(C) As in (B), but showing the primary sequence of human SHH.

(D) Testing SHH-NL fusions for SCUBE2-dependent release. SHH-NL fusions were co-transfected with SCUBE2 or the inactive SCUBE2-ty97 mutant (Hollway et al., 2006; Kawakami et al., 2005; Woods and Talbot, 2005) in HEK293T cells, and release into serum-free media was assayed by luminescence in a single replicate. The fusions SHH-NL5, SHH-NL7 and SHH-NL9 are released in a SCUBE2-dependent manner.

(E) Tagged mouse SCUBE2 was stably expressed in HEK293S cells, and was affinity purified from conditioned media. Purified SCUBE2 was analyzed by SDS-PAGE, followed by Coomassie staining.

(F) Kinetics of SHH-NL5 and SHH-NL7 release. Cells stably expressing SHH-NL5 or SHH-NL7 were incubated with purified recombinant SCUBE2 (300nM), in the presence of the protein synthesis inhibitor, cycloheximide (100µg/mL). At the indicated times, SHH-NL5 or SHH-NL7 released into serum-free media was measured by NanoLuc luminescence assay in a single replicate. Incubation with BSA (300nM) served as negative control.

(G) Cell lysates from stable cell lines used in Figure 1E. HEK293T cells stably expressing SHH-NL5 or SHH were analyzed by immunoblotting. Precursor and processed forms are indicated for each protein.

(H) Cell lines from (G) were incubated with purified SCUBE2 (500nM), and SHH release was measured by immunoblotting. Release by bovine serum albumin (BSA, 500nM) served as negative control. SCUBE2 released SHH-NL5 and SHH with similar kinetics and in similar amounts, when adjusted for expression levels in lysates (G). See Figure 1E for quantification.

(I) As in (H), but measuring SHH-NL5 release by NanoLuc luminescence assay.

(J) As in (H), but showing correlation between SHH-NL5 release as measured by densitometry and by luminescence. The two measurements show strong linear correlation. Curve shows linear fit with associated confidence envelope shown by dotted lines.

Figure S2

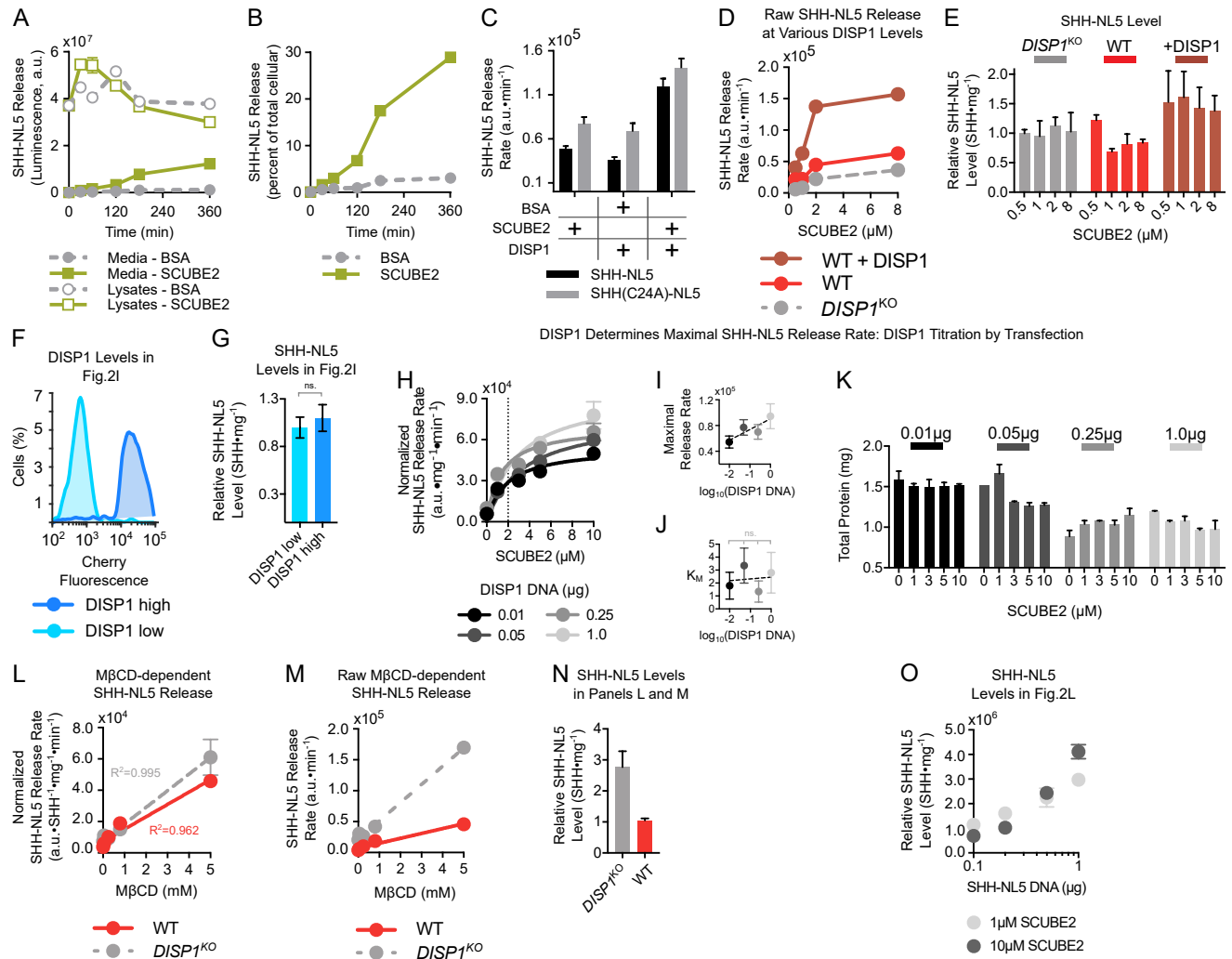


Figure S2. Kinetics of catalyzed and uncatalyzed SHH-NL5 release, related to Figure 2

(A) Cells stably expressing SHH-NL5 were incubated with purified SCUBE2 (1μM), in the presence of CHX (100μg/mL). At the indicated times, both SHH-NL5 released into the media and SHH-NL5 left in the cells were measured in a single replicate. At times <2 hours, released SHH-NL5 represents a very small fraction of cellular SHH-NL5, indicating that SHH-NL5 levels are not limiting for DISP1- and SCUBE2-dependent release. Incubation with BSA (1μM) was used as negative control.

(B) As in (A), but showing the percentage of total SHH-NL5 released into the media.

(C) SHH-NL5 or SHH(C24A)-NL5 was stably expressed in *DISP1*^{KO} cells, and initial SHH-NL5 release rates were measured for cells treated with purified SCUBE2 (1μM) or BSA (1μM), with or without transient DISP1 expression. SHH(C24A)-NL5, which is modified with cholesterol but not palmitate, is still released in a DISP1- and SCUBE2-dependent manner. Data show estimates of release rate, and error bars show standard error of the estimate.

(D) Graph showing pre-normalization SHH-NL5 release rates for the experiment in Figure 2F.

(E) Graph showing relative SHH-NL5 levels across cell lines, measured as luminescence per total protein (mg), for the experiment in Figure 2F. Error bars show standard deviation around the mean.

(F) DISP1 levels in cells expressing high and low levels of DISP1, related to Figure 2I. Cells stably expressing SHH-NL5 and mCherry-tagged DISP1 were sorted into populations expressing high or low levels of DISP1, based on mCherry fluorescence. Curves show fluorescence distributions for each population after fluorescence-activated cell sorting.

(G) Graph showing relative SHH-NL5 levels across cell lines, measured as luminescence per cell number (total protein (mg)), for the experiment in Figure 2I. Error bars show standard deviation around the mean.

(H) SHH-NL5 initial release rates plotted as function of SCUBE2 concentration for *DISP1*^{KO} cells transiently transfected with different amounts of wild-type DISP1 in single replicates. Data show release rate estimates; error bars show standard error of the estimate; curves show fits to the Michaelis–Menten equation. Initial release rates were normalized to SHH-NL5 expression levels in each cell line, and to total cell number (total protein) in each experimental condition. SHH-NL5 initial release rates increase with increasing DISP1 levels, while displaying saturation relative to SCUBE2. Vertical dotted line shows K_M estimate.

(I) Estimates of V_{max} for the indicated conditions in (H). Error bars indicate standard error of the estimate.

(J) Estimates of K_M for the indicated conditions in (H). Error bars indicate standard error of the estimate. ns. – not statistically significant, two-tailed t-test, $p < 0.05$.

(K) Graph showing total protein across conditions, for the experiment in (H). Error bars show standard deviation around the mean.

(L) SHH-NL5 was stably expressed in wild-type or *DISP1*^{KO} cells, and initial SHH-NL5 release rates were measured for various concentrations of added methyl- β -cyclodextrin (M β CD) in single replicates. Rates were normalized to SHH-NL5 expression levels in each cell line, and to the cell number in each experimental condition (total protein (mg)). Data show release rate estimates; error bars show standard error of the estimate; curves show linear fits with associated R² values. SHH-NL5 release by M β CD obeys simple mass-action kinetics, does not require DISP1, and does not saturate, in contrast to DISP1-catalyzed release by SCUBE2.

(M) Graph showing pre-normalization SHH-NL5 release rates for the experiment in (L).

(N) Graph showing relative SHH-NL5 levels across cell lines, as luminescence per total protein (mg), for the experiment in (L). Data show mean of two replicates and error bars show standard deviation around the mean.

(O) Graph showing relative SHH-NL5 levels, as luminescence per total protein (mg), for the experiment in [Figure 2L](#), as a function of transfected DNA. Data show mean level; error bars show standard deviation around the mean.

Figure S3

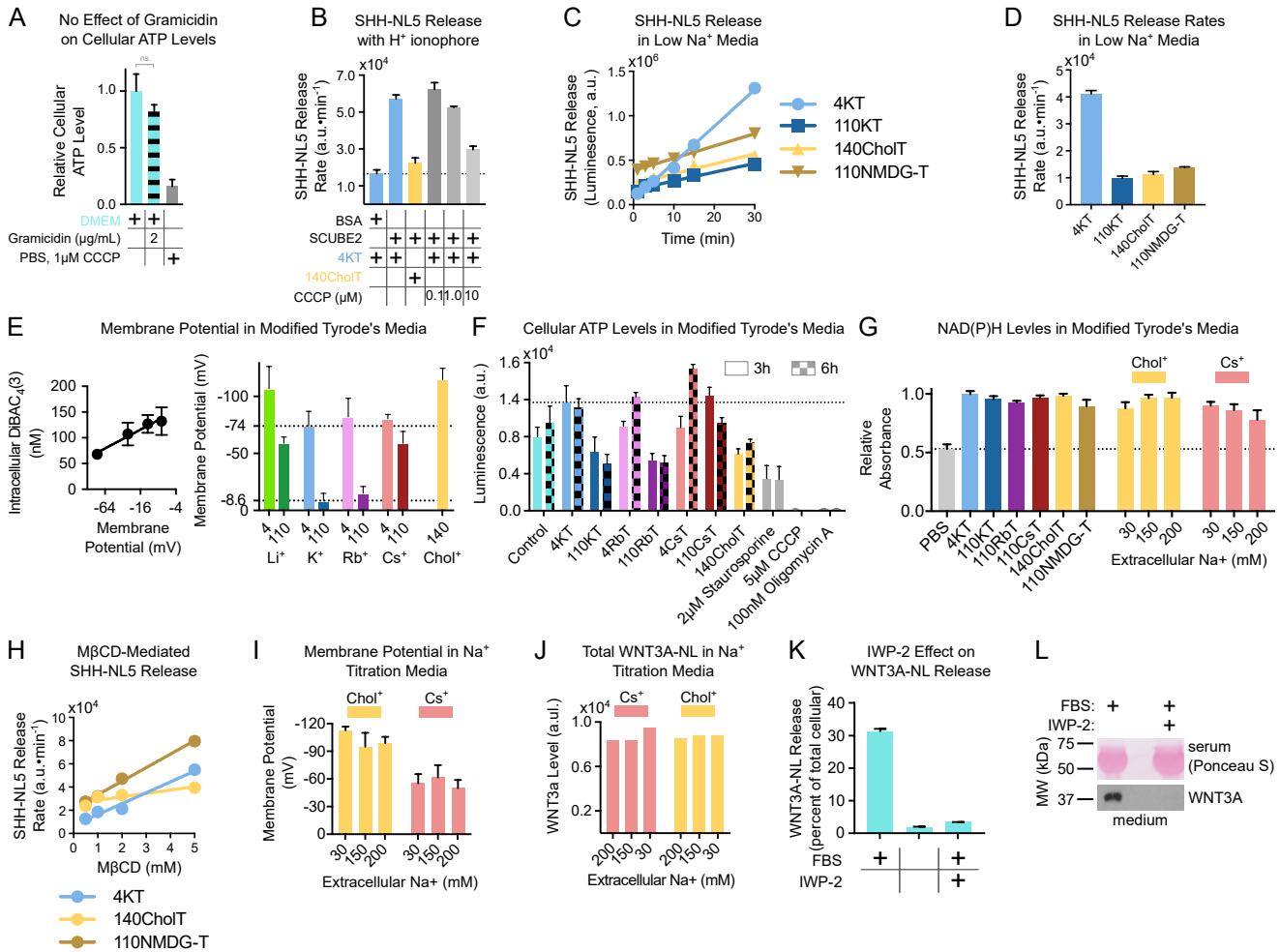


Figure S3. Role of the Na⁺ gradient in DISP1-dependent and DISP1-independent SHH-NL5 release, related to Figure 3

(A) Cellular ATP levels in cells treated for 30min with gramicidin (2µg/mL), related to Figure 3B. Incubation with CCCP serves as a positive control for ATP depletion. Data show mean of four replicates and error bars represent standard deviation around the mean.

(B) Cells stably expressing SHH-NL5 were incubated with SCUBE2 (1µM) in Tyrode's media (4KT), in the absence or presence of the H⁺-specific ionophore CCCP, or in media in which Na⁺ was replaced by choline⁺ (140ChoIT). Protein synthesis was inhibited with CHX (100µg/mL). Released SHH-NL5 was measured by NanoLuc luminescence assay in a single replicate. SHH-NL5 release is unaffected by up to 1µM CCCP. Error bars show standard error of the estimated release rates.

(C) As in (B), but cells were incubated in Tyrode's media containing physiological Na⁺ levels (4KT), or media in which Na⁺ was replaced by K⁺, choline⁺, or NMDG⁺ (110KT, 140ChoIT, 110NMDG-T). SHH-NL5 release is inhibited in low Na⁺ media. Curves show linear fits to release data in single replicate.

(D) Graph showing SHH-NL5 release rates for the experiment in (C). Error bars show standard error of the estimate.

(E) Membrane potential of cells incubated in various media, measured by DiBAC₄(3) accumulation. Left: media with varying concentrations of K⁺ were used to generate a standard curve, to calculate E_m from DiBAC₄(3) fluorescence intensity, using the Nernst equation. Right: high K⁺ and Rb⁺ depolarize the cells, while Li⁺, Cs⁺ and choline⁺ do not. Error bars represent standard deviations around the mean of three biological replicates.

(F) Cellular ATP levels in cells incubated in the indicated media for 3 or 6 hours. Incubation with staurosporine, CCCP, or oligomycin A served as positive controls for ATP depletion. Error bars represent standard deviation around the mean of three biological replicates.

(G) NAD(P)H levels in cells incubated in the indicated media for 3 hours. NAD(P)H levels were measured using an MTT viability assay in triplicate. Incubation in PBS was used as a positive control. Error bars represent standard deviation around the mean.

(H) As in (C), but measuring initial rates of SHH-NL5 release by varying MβCD concentrations. Extracellular Na⁺ is dispensable for SHH-NL5 release by MβCD, which is linear with respect to MβCD, in contrast to DISP1- and SCUBE2-dependent release, which is hyperbolic with respect to SCUBE2 and SHH-NL5. Curves show linear fits with R²=0.976, R²=0.821, and R²=0.996 for 4KT, 140ChoIT, and 110NMDG-T respectively.

(I) As in (E), but measuring the membrane potential in media of varying Na⁺ concentration, related to Figure 3E-I. Altering Na⁺ concentration in each medium does not change the membrane potential. Error bars represent standard deviation around the mean of three biological replicates.

(J) Total WNT3A-NL released for the experiment in Figure 3H. Single replicate.

(K) WNT3A-NL was stably expressed in L cells, and its release was assayed, in triplicate, after overnight incubation in the absence or presence of serum (FBS, 10%), and in the absence or presence of IWP-2 (2µM), which blocks WNT palmitoylation by Porcupine (PORCN). WNT3A-NL release occurs in media supplemented with serum, but not in the absence of serum. WNT3A-NL secretion is palmitoylation-dependent.

(L) As in (K), but with stably expressed untagged WNT3A. WNT3A was visualized by immunoblotting. Serum protein was visualized by Ponceau S staining. WNT3A secretion is serum- and palmitoylation-dependent.

Figure S4

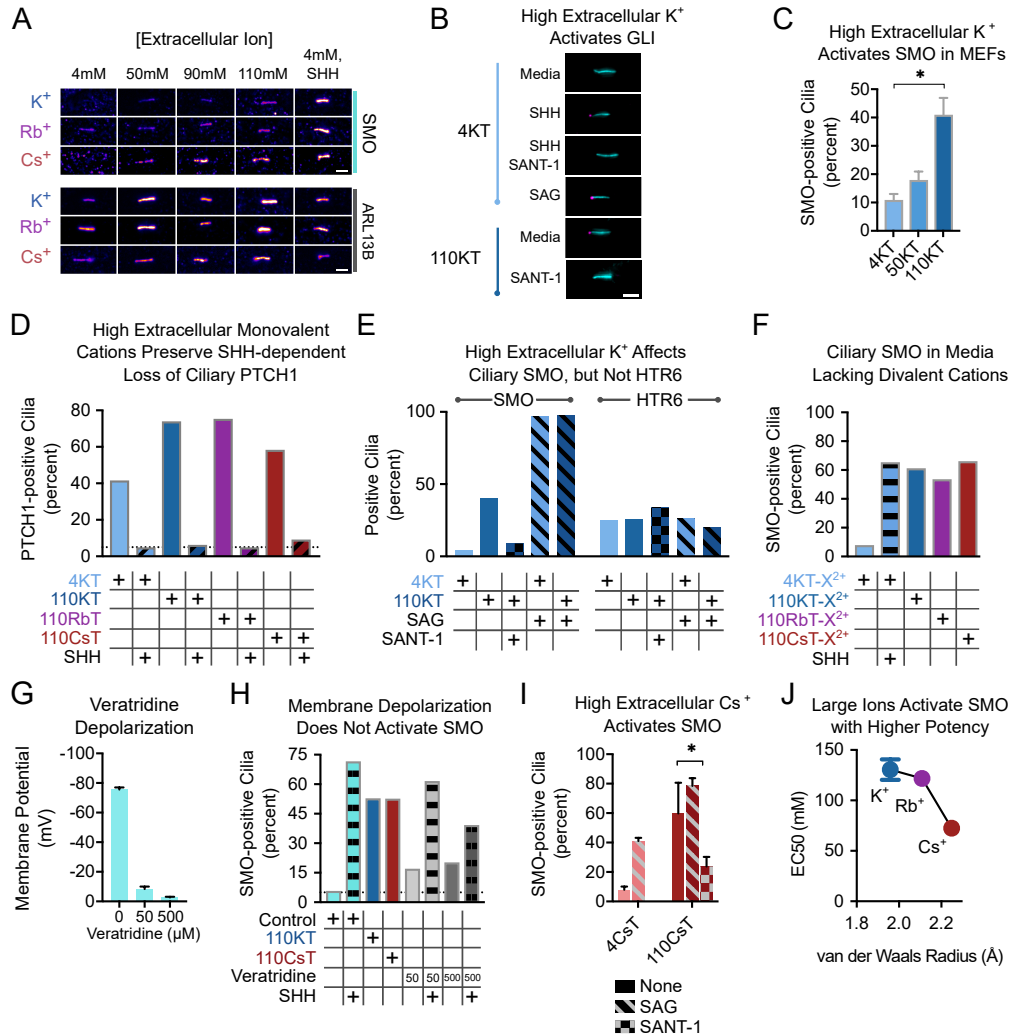


Figure S4. Role of K⁺ gradient for PTCH1 function, related to Figure 5

(A) Representative immunofluorescence micrographs of cilia for the experiment in Figure 5B. SHH was used as positive control for SMO activation. High extracellular concentrations of K⁺, Rb⁺, or Cs⁺ lead to SMO accumulation in cilia. Scale bar = 2 μm.

(B) Representative immunofluorescence micrographs of cilia for the experiment in Figure 5C. GLI is shown in magenta, while the ciliary marker acetylated tubulin (AcTub) is shown in teal. Media with high K⁺ causes GLI accumulation in cilia, which is reversed by SANT-1 (1 μM). SHH and SAG were used as positive controls. Scale bar = 2 μm.

(C) Confluent mouse embryonic fibroblast (MEF) cultures were serum-starved overnight, to promote ciliogenesis, and were then incubated for 3 hours in isotonic Tyrode's media with increasing concentrations (4, 50, 110mM) of K⁺ instead of Na⁺ (4KT, 50KT, 110KT). Endogenous SMO at cilia was measured by immunofluorescence microscopy. ARL13B was used as ciliary marker. High extracellular K⁺ causes SMO accumulation in cilia. Error bars represent standard deviation around the mean of two biological replicates; at least 100 cilia were assayed per replicate. * p<0.05, unpaired, two-tailed t-test.

(D) Graph showing percentage of PTCH1-positive cilia for the experiment in Figure 5F. Single replicate.

(E) Ciliated NIH-3T3 cells stably expressing HA-tagged serotonin receptor 6 (HTR6) were incubated for 3 hours in the indicated media. HTR6 and endogenous SMO levels in cilia were measured by immunofluorescence. High extracellular K⁺ recruits SMO to cilia, but does not perturb ciliary localization of HTR6. SMO recruitment is reversed by SANT-1 (1 μM). SAG (500nM) was used as positive control for SMO activation. At least 100 cilia were measured per condition in a single replicate.

(F) As in (E), but measuring ciliary SMO in NIH-3T3 cells incubated in modified Tyrode's media lacking divalent cations. SHH was used as positive control for SMO activation. At least 100 cilia were assayed per condition in a single replicate.

(G) Membrane potential in cells treated with the voltage-gated sodium channel agonist veratridine. Veratridine efficiently depolarizes cells. Error bars represent standard deviation around the mean of three biological replicates.

(H) As in (F), but cells were depolarized with the Na⁺-channel agonist veratridine (50 or 500 μM). Membrane depolarization by veratridine does not appreciably elevate ciliary SMO levels. Cells incubated with veratridine still respond to SHH. At least 100 cilia were assayed per condition in a single replicate.

(I) Ciliated NIH-3T3 cells were incubated for 3 hours in isotonic media with low (4CsT) or high (110CsT) Cs⁺, and endogenous SMO at cilia was measured by immunofluorescence in triplicate. SMO accumulates in cilia in 110CsT media, which is reversed by SANT-1. Treatment with SAG serves as positive control. Error bars show standard deviation around the mean; * p<0.05, unpaired, two-tailed t-test.

(J) EC50 values from the experiment in Figure 5B plotted as function of ionic van der Waals radius. Larger monovalent cations are more potent at inducing SMO ciliary accumulation. Error bars show standard error of the estimate.

Figure S5

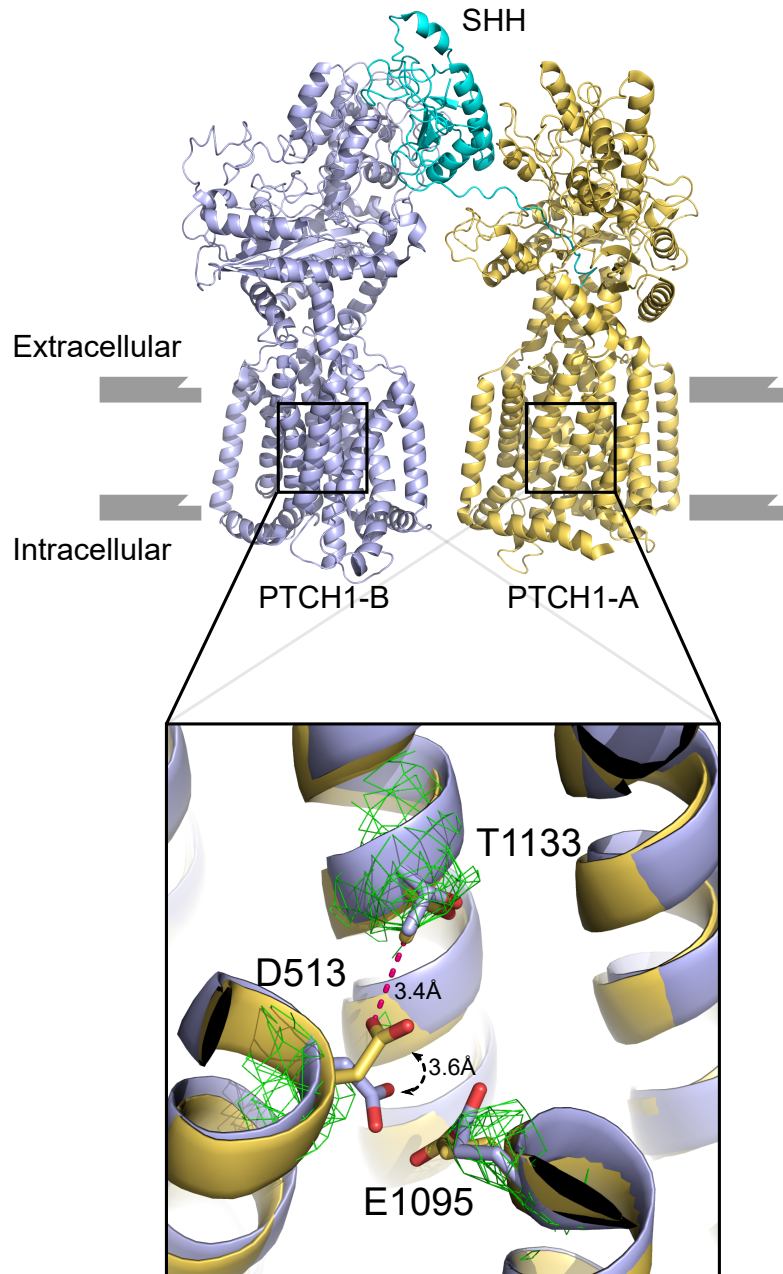


Figure S5. Evidence for an alternating hydrogen-bonding network in the transmembrane domain of PTCH1, related to Figure 6

Cryo-EM structure of SHH (teal) bound to two molecules of human PTCH1 (PDB: 6e1h), shown in yellow (PTCH1-A protomer) and purple (PTCH1-B protomer). The inset shows a close-up view of the superimposed TM regions of the two PTCH1 protomers. In protomer A, the residue D513 in TM4 appears to form a hydrogen bond with residue T1133 in TM11. Movement of D513 breaks the hydrogen bond in protomer B. Green mesh shows cryo-EM map around the indicated residues, contoured at 5σ .

Figure S6

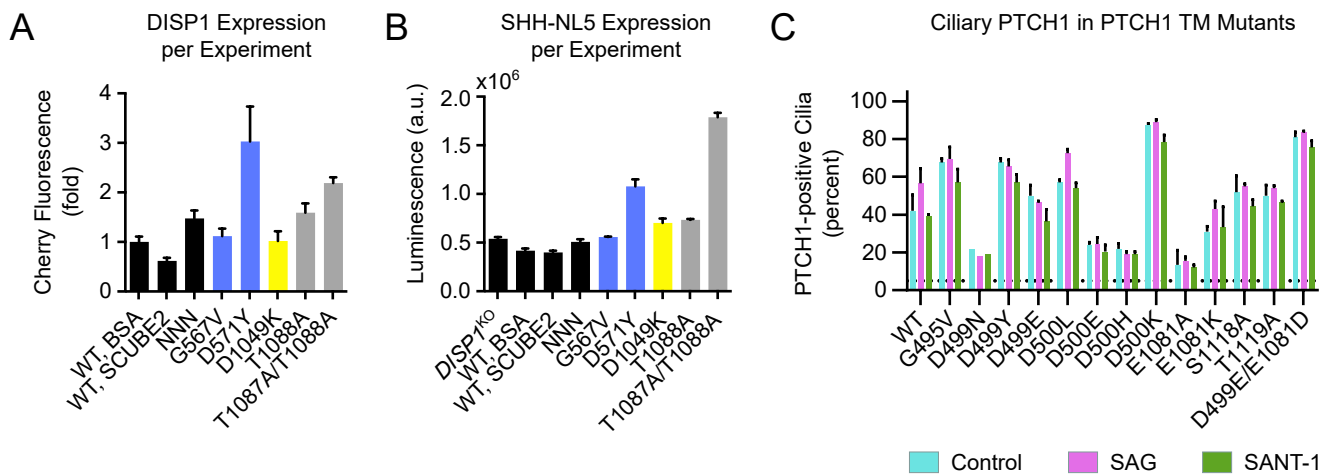


Figure S6. Characterization of stable cell lines used for DISP1 and PTCH1 mutant analysis, related to Figure 6

(A) Graph showing relative DISP1-mCherry expression level across cell lines, measured as mCherry fluorescence per cell number (total protein) for the experiment in Figure 6D. Error bars show standard deviation around the mean of technical triplicates.

(B) Graph showing relative SHH-NL5 expression level across cell lines, measured as luminescence per cell number (total protein), for the experiment in Figure 6D. Error bars show standard deviation around the mean of technical triplicates.

(C) Graph showing that PTCH1 mutants localize to cilia, measured as percentage of PTCH1-positive (mCherry-positive) cilia for the experiment in Figure 6E. Error bars show standard deviation around the mean of two biological replicates.

Table S1. Composition of modified Tyrode's media, related to STAR Methods

Media	Buffer	[Na ⁺]	[Li ⁺ /K ⁺ /Rb ⁺ /Cs ⁺ / Choline ⁺ /NMDG ⁺]	[Cl ⁻]	[Glucose]	[Mg ²⁺]	[Ca ²⁺]	[HCO ₃ ⁻]	Osmolarity
4LiT	10mM Na-Hepes pH7.5	110mM	4mM Li ⁺ 50mM Choline ⁺	120mM	10mM	2mM	2mM	30mM	300 mOsmol/L
110LiT	10mM Na-Hepes pH7.5	10mM	110mM Li ⁺ 40mM Choline ⁺	110mM	10mM	2mM	2mM	30mM	300 mOsmol/L
4KT	10mM Na-Hepes pH7.5	110mM	4mM K ⁺ 50mM Choline ⁺	120mM	10mM	2mM	2mM	30mM	300 mOsmol/L
50KT	10mM Na-Hepes pH7.5	60mM	50mM K ⁺ 50mM Choline ⁺	120mM	10mM	2mM	2mM	30mM	300 mOsmol/L
90KT	10mM Na-Hepes pH7.5	20mM	90mM K ⁺ 50mM Choline ⁺	120mM	10mM	2mM	2mM	30mM	300 mOsmol/L
110KT	10mM Na-Hepes pH7.5	10mM	110mM K ⁺ 50mM Choline ⁺	110mM	10mM	2mM	2mM	30mM	300 mOsmol/L
4RbT	10mM Na-Hepes pH7.5	110mM	4mM Rb ⁺ 50mM Choline ⁺	120mM	10mM	2mM	2mM	30mM	300 mOsmol/L
50RbT	10mM Na-Hepes pH7.5	60mM	50mM Rb ⁺ 50mM Choline ⁺	120mM	10mM	2mM	2mM	30mM	300 mOsmol/L
90RbT	10mM Na-Hepes pH7.5	20mM	90mM Rb ⁺ 50mM Choline ⁺	120mM	10mM	2mM	2mM	30mM	300 mOsmol/L
110RbT	10mM Na-Hepes pH7.5	10mM	110mM Rb ⁺ 50mM Choline ⁺	110mM	10mM	2mM	2mM	30mM	300 mOsmol/L
4CsT	10mM Na-Hepes pH7.5	110mM	4mM Cs ⁺ 50mM Choline ⁺	120mM	10mM	2mM	2mM	30mM	300 mOsmol/L
50CsT	10mM Na-Hepes pH7.5	60mM	50mM Cs ⁺ 50mM Choline ⁺	120mM	10mM	2mM	2mM	30mM	300 mOsmol/L
90CsT	10mM Na-Hepes pH7.5	20mM	90mM Cs ⁺ 50mM Choline ⁺	120mM	10mM	2mM	2mM	30mM	300 mOsmol/L
110CsT	10mM Na-Hepes pH7.5	10mM	110mM Cs ⁺ 50mM Choline ⁺	110mM	10mM	2mM	2mM	30mM	300 mOsmol/L
110NMDG-T	10mM Na-Hepes pH7.5	10mM	4mM K ⁺ 110mM NMDG ⁺	110mM	10mM	2mM	2mM	30mM	300 mOsmol/L
140CholineT	10mM Na-Hepes pH7.5	10mM	140mM Choline ⁺	110mM	10mM	2mM	2mM	30mM	300 mOsmol/L
4KT-X ²⁺	10mM Na-Hepes pH7.5	110mM	4mM K ⁺ 50mM Choline ⁺	120mM	10mM	0mM	0mM	30mM	300 mOsmol/L
110KT-X ²⁺	10mM Na-Hepes pH7.5	10mM	110mM K ⁺ 50mM Choline ⁺	110mM	10mM	0mM	0mM	30mM	300 mOsmol/L
110RbT-X ²⁺	10mM Na-Hepes pH7.5	10mM	110mM Rb ⁺ 50mM Choline ⁺	110mM	10mM	0mM	0mM	30mM	300 mOsmol/L
110CsT-X ²⁺	10mM Na-Hepes pH7.5	10mM	110mM Cs ⁺ 50mM Choline ⁺	110mM	10mM	0mM	0mM	30mM	300 mOsmol/L

Table S2. Generation of *DISP1*^{KO} HEK293T cells, related to STAR Methods

gRNA Oligonucleotides

gRNA ID	Target Gene	gRNA #	NCBI Reference Sequence	Target Site	gRNA Sequence	gRNA Orientation	Associated Plasmid
hDISP1_KO_gRNA1	<i>DISP1</i>	1	NM_001369594.1	Exon 2	TGACCGTGCCATTAAGTTGC	antisense	pBMW275
hDISP1_KO_gRNA2	<i>DISP1</i>	2	NM_001369594.1	Exon 4	GGCACAGACTACGATGAACA	antisense	pBMW276

CRISPR Sequencing Primers

Primer ID	Target Gene	gRNA #	Direction	Barcode Sequence	Target Recognition Sequence
PR8.E2	<i>DISP1</i>	1	forward	ACACTCTTTCCCTACACGACGCTCTTCCGATCT	CCTGTGATGGAGACCATGC
PR8.E3	<i>DISP1</i>	1	reverse	GTGACTGGAGTTCAGACGTGTGCTCTTCCGATCT	GGCTAGTCAAAGGGTGATGGTA
PR8.E4	<i>DISP1</i>	2	forward	ACACTCTTTCCCTACACGACGCTCTTCCGATCT	CCGACACTTCTTTGTGTTTTGT
PR8.E5	<i>DISP1</i>	2	reverse	GTGACTGGAGTTCAGACGTGTGCTCTTCCGATCT	CAATATTTGGAGATGATTTTAGGCT

Lesions Present in *DISP1*^{KO} Cells

gRNA #	Allele 1 Sequence	Allele 1 Type	Allele 1 % Aligned Reads	Allele 2 Sequence	Allele 2 Type	Allele 2 % Aligned Reads
1	GCA-[T]TTAATGGCACGGTCA	1-nt deletion; transition	50	GCA-----CGGTCA	11-nt deletion	50
2	T--TCATCGTAGTCTGTGCC	2-nt deletion	100			
Deletion	GCA//TCATCGTAGTCTGTGCC	47687-nt deletion	100			

Two gRNAs were used simultaneously, producing one fused deletion allele as well as additional alleles with frameshifts at each gRNA locus, suggesting that three copies of the *DISP1* locus are present in this line.

Table S3. List of plasmids used in this study, related to STAR Methods

pBMW Identifier	Vector	Promoter	Short Name	Full Transgene	Euk. Marker	Bact. Marker	Category	Subcategory
pAS1	pCS2	IE94-CMV	SHH	hSHH-FL	--	Amp	transient expression	SHH release
pBMW146	pCS2	IE94-CMV	SCUBE2	HA-mSCUBE2-Del(Furin)	--	Amp	transient expression	SHH release; positive control
pBMW157	pCS2	IE94-CMV	SCUBE2-ty97	HA-mSCUBE2-Del(CUB)	--	Amp	transient expression	SHH release; negative control
pAS64	pCS2	IE94-CMV	DISP1-WT	mDISP1::fEGFP	--	Amp	transient expression	DISP1 rescue; positive control
pAS65	pCS2	IE94-CMV	DISP1-NNN	mDISP1(D571N,D572N,D1049N)::fEGFP	--	Amp	transient expression	DISP1 rescue; negative control
pAS123	pCS2	IE94-CMV	NL1	hSHH(NanoLuc1)-FL	--	Amp	transient expression	screening for NL insertion sites
pAS124	pCS2	IE94-CMV	NL2	hSHH(NanoLuc2)-FL	--	Amp	transient expression	screening for NL insertion sites
pAS125	pCS2	IE94-CMV	NL3	hSHH(NanoLuc3)-FL	--	Amp	transient expression	screening for NL insertion sites
pAS126	pCS2	IE94-CMV	NL4	hSHH(NanoLuc4)-FL	--	Amp	transient expression	screening for NL insertion sites
pAS127	pCS2	IE94-CMV	NL5	hSHH(NanoLuc5)-FL	--	Amp	transient expression	screening for NL insertion sites
pAS128	pCS2	IE94-CMV	NL6	hSHH(NanoLuc6)-FL	--	Amp	transient expression	screening for NL insertion sites
pAS129	pCS2	IE94-CMV	NL7	hSHH(NanoLuc7)-FL	--	Amp	transient expression	screening for NL insertion sites
pAS130	pCS2	IE94-CMV	NL8	hSHH(NanoLuc8)-FL	--	Amp	transient expression	screening for NL insertion sites
pAS131	pCS2	IE94-CMV	NL9	hSHH(NanoLuc9)-FL	--	Amp	transient expression	screening for NL insertion sites
pAS77	pHAGE2	CAG-CMV	DISP1	mDISP1::fmCherry	Blast	Amp	transient expression	testing role of DISP1 dose on SHH release
pBMW275	pX330	U6	--	hDISP1_CRISPR_KO_gRNA1	--	Amp	CRISPR knockout generation	DISP1
pBMW276	pX330	U6	--	hDISP1_CRISPR_KO_gRNA2	--	Amp	CRISPR knockout generation	DISP1
pAS296	pHAGE2	EF1 α	--	hSHH	Puro	Amp	stable mammalian expression	SHH
pAS144	pHAGE2	CAG-CMV	--	hSHH(NanoLuc5)-FL	Puro	Amp	stable mammalian expression	SHH-NL

pBMW Identifier	Vector	Promoter	Short Name	Full Transgene	Euk. Marker	Bact. Marker	Category	Subcategory
pAS145	pHAGE2	CAG-CMV	--	hSHH(NanoLuc7)-FL	Puro	Amp	stable mammalian expression	SHH-NL
pAS258	pHAGE2	CAG-CMV	--	hSHH(C24A; NanoLuc5)-FL	Puro	Amp	stable mammalian expression	SHH-NL
pAS77	pHAGE2	CAG-CMV	--	mDISP1::fmCherry	Blast	Amp	stable mammalian expression	DISP1 variants
pAS78	pHAGE2	CAG-CMV	--	mDISP1(D571N,D572N,D1049N)::fmCherry	Blast	Amp	stable mammalian expression	DISP1 variants
pBMW479	pHAGE2	CAG-CMV	--	mDISP1(G567V)::fmCherry	Blast	Amp	stable mammalian expression	DISP1 variants
pBMW480	pHAGE2	CAG-CMV	--	mDISP1(D571Y)::fmCherry	Blast	Amp	stable mammalian expression	DISP1 variants
pBMW481	pHAGE2	CAG-CMV	--	mDISP1(D1049K)::fmCherry	Blast	Amp	stable mammalian expression	DISP1 variants
pBMW483	pHAGE2	CAG-CMV	--	mDISP1(T1088A)::fmCherry	Blast	Amp	stable mammalian expression	DISP1 variants
pBMW484	pHAGE2	CAG-CMV	--	mDISP1(T1087,1088A)::fmCherry	Blast	Amp	stable mammalian expression	DISP1 variants
pAS297	pHAGE2	CAG-CMV	--	FLAG-NanoLuc::mWNT3A	Blast	Amp	stable mammalian expression	WNT3A-NL
pKP4	pHAGE2	CAG-CMV	--	mPTCH1::fmCherry	Blast	Amp	stable mammalian expression	PTCH1 variants
pKP5	pHAGE2	CAG-CMV	--	mPTCH1(G495V)::fmCherry	Blast	Amp	stable mammalian expression	PTCH1 variants
pKP6	pHAGE2	CAG-CMV	--	mPTCH1(D499N)::fmCherry	Blast	Amp	stable mammalian expression	PTCH1 variants
pKP7	pHAGE2	CAG-CMV	--	mPTCH1(D499Y)::fmCherry	Blast	Amp	stable mammalian expression	PTCH1 variants
pKP8	pHAGE2	CAG-CMV	--	mPTCH1(D499E)::fmCherry	Blast	Amp	stable mammalian expression	PTCH1 variants
pKP9	pHAGE2	CAG-CMV	--	mPTCH1(D500L)::fmCherry	Blast	Amp	stable mammalian expression	PTCH1 variants
pKP10	pHAGE2	CAG-CMV	--	mPTCH1(D500E)::fmCherry	Blast	Amp	stable mammalian expression	PTCH1 variants
pKP11	pHAGE2	CAG-CMV	--	mPTCH1(D500H)::fmCherry	Blast	Amp	stable mammalian expression	PTCH1 variants
pKP12	pHAGE2	CAG-CMV	--	mPTCH1(D500K)::fmCherry	Blast	Amp	stable mammalian expression	PTCH1 variants
pKP13	pHAGE2	CAG-CMV	--	mPTCH1(E1081A)::fmCherry	Blast	Amp	stable mammalian expression	PTCH1 variants

pBMW Identifier	Vector	Promoter	Short Name	Full Transgene	Euk. Marker	Bact. Marker	Category	Subcategory
pKP14	pHAGE2	CAG-CMV	--	mPTCH1(E1081K)::fmCherry	Blast	Amp	stable mammalian expression	PTCH1 variants
pKP15	pHAGE2	CAG-CMV	--	mPTCH1(S1118A)::fmCherry	Blast	Amp	stable mammalian expression	PTCH1 variants
pKP16	pHAGE2	CAG-CMV	--	mPTCH1(T1119A)::fmCherry	Blast	Amp	stable mammalian expression	PTCH1 variants
pKP17	pHAGE2	CAG-CMV	--	mPTCH1(D499E,E1081D)::fmCherry	Blast	Amp	stable mammalian expression	PTCH1 variants
pBMW153	pHAGE2	CAG-CMV	--	FLAG-HT7-Presci::mSCUBE2-Del(Furin)	Blast	Amp	stable mammalian protein production	SCUBE2 protein